JPL PUBLICATION 80-66

(NASA-CR-163745) ROTATING LIQUID DROPS: PLATEAUS EXPERIMENT REVISITED (Jet Propulsion Lab.) 71 p HC A04/MF A01 CSCL 20D

N81-12357

Unclas
G3/34 29311

Rotating Liquid Drops: Plateau's Experiment Revisited

R. Tagg
L. Cammack
A. Croonquist
T. G. Wang

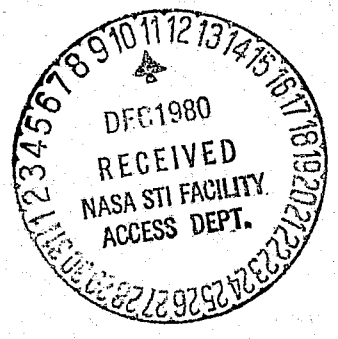

October 15, 1980

National Aeronautics and
Space Administration

Jet Propulsion Laboratory
California Institute of Technology
Pasadena, California

TECHNICAL REPORT STANDARD TITLE PAGE

1. Report No. 80-66	2. Government Accession No.	3. Recipient's Catalog No.
4. Title and Subtitle Plateau's Experiment Revisited		5. Report Date 10-15-80 6. Performing Organization Code
7. Author(s) T. Wang		8. Performing Organization Report No.
9. Performing Organization Name and Address JET PROPULSION LABORATORY California Institute of Technology 4800 Oak Grove Drive Pasadena, California 91103		10. Work Unit No. 11. Contract or Grant No. NAS 7-100 13. Type of Report and Period Covered JPL Publication
12. Sponsoring Agency Name and Address NATIONAL AERONAUTICS AND SPACE ADMINISTRATION Washington, D.C. 20546		14. Sponsoring Agency Code
15. Supplementary Notes		

16. Abstract

The dynamics of liquid drops rotating in another liquid has been studied experimentally with an oil drop suspended in a neutral buoyancy tank. New stable shapes not predicted by the theory have been observed.

17. Key Words (Selected by Author(s))	18. Distribution Statement
Physics Fluid Mechanics Wave Propagation Astrophysics	Unclassified - Unlimited

19. Security Classif. (of this report)	20. Security Classif. (of this page)	21. No. of Pages	22. Price
Unclassified	Unclassified	72	

JPL PUBLICATION 80-66

Rotating Liquid Drops: Plateau's Experiment Revisited

R. Tagg
L. Cammack
A. Croonquist
T. G. Wang

October 15, 1980

National Aeronautics and
Space Administration

Jet Propulsion Laboratory
California Institute of Technology
Pasadena, California

CONTENTS

Figures

Figures (Continued)

Figures (Continued)

ABSTRACT

The dynamics of liquid drops rotating in another liquid has been studied experimentally with an oil drop suspended in a neutral buoyancy tank. New stable shapes not predicted by the theory have been observed.

SECTION I

INTRODUCTION

This paper describes the recent investigations of the dynamics of a liquid mass rotating under the influence of surface tension.

This experiment, devised by J. Plateau[1] in the last century, is being repeated at JPL. Recent theoretical developments in this area, and the advancements in photographic and electronic systems since Plateau's time, provide motivation to repeat the experiment in a much more controlled manner. Thus, this experiment provides a quantitative comparison with the theory. Furthermore, it serves as a precursor to flight experiments to be conducted in weightlessness aboard the Space Shuttle[2].

A large ($\sim$15 cc), viscous liquid drop is formed around a disc and shaft in a tank containing a much less viscous mixture having the same density as the drop, as shown in Figure 1-1. This supporting liquid and the drop are immiscible. If the shaft and disc were not present, the drop would float freely in the surrounding medium and assume the shape of a sphere. The gravitational forces this drop feels are small, much less than the surface forces. With the drop attached and initially centered about the disc, the shaft and disc are set into rotation almost impulsively, reaching a final steady angular velocity within one-half to two revolutions. The drop deforms under rotation and develops into a variety of shapes depending on the shaft velocity. The process of spin-up, development, and decay (or fracture) to some final shape is recorded on motion picture film.

In this system, gravity is diminished at the expense of introducing a supporting liquid which is viscous and may be entrained by the motion of the drop, thereby allowing angular momentum to be transferred from the drop. Rotation is achieved only by introducing the shaft and disc; adhesion to these surfaces distorts the drop's shape. Nevertheless, comparison of this experiment's results to the theory of free rotating liquid drops is prompted by the fact that several novel families of drop shapes have been observed.

It is important to recognize that existing theory deals mainly with equilibrium shapes and their stability, while the drop in this experiment is undergoing a far more complicated process. The shape of a liquid drop spun on a shaft and supported by another liquid is very much a dynamical problem. A proper understanding of the results will only come with a dynamical analysis which succeeds in explaining the growth and decay versus time of the various drop shapes.

Page intentionally left blank

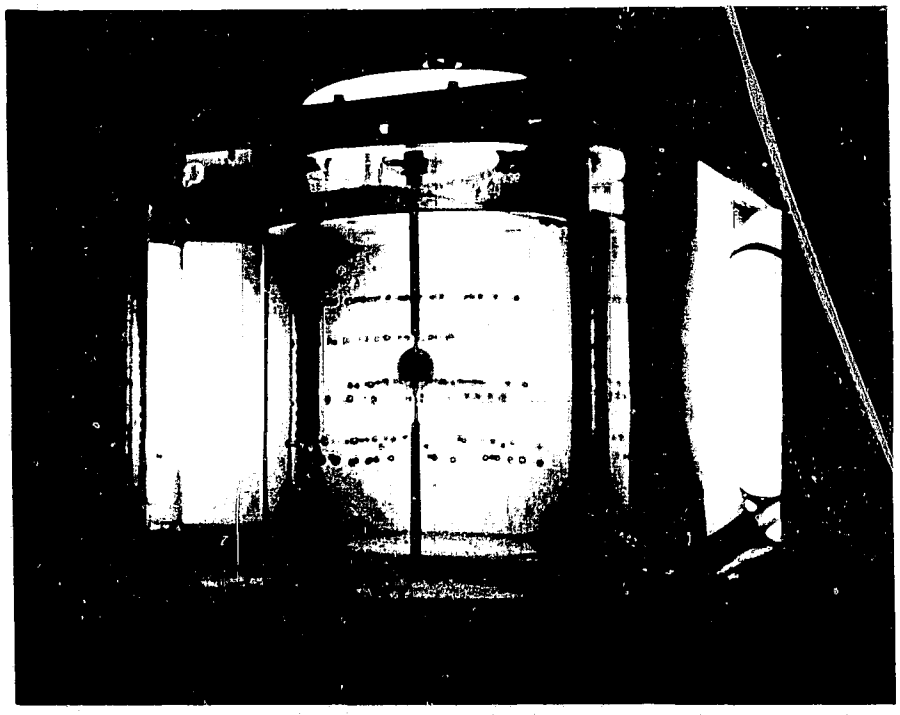

Figure I-1. The Neutral Buoyancy Tank. (The several layers of test drops of different colors and densities show the existence of a density gradient in the tank. Each layer of test drops is neutrally buoyant with the outer fluid at a definite height.) During experimental runs, the large drop is centered about the disc.

I-2

SECTION II

THEORY

Results from the theory[4-11] of free rotating drops are discussed below with the understanding that this theory describes a system which, in many ways, is significantly different from the neutral-buoyancy system. Several excellent reviews already exist[4,5,11]; for the most part they will not be duplicated here.

Swiatecki[4] fits the problem of a liquid drop held together by surface tension into a broader scheme in which fluid masses may, in addition to having surface tension, be self-gravitating and/or possess a uniform density of electric charge. The astrophysical problem of the stability of rotating, self-gravitating stellar masses, and the problem of the fissionability of rotating uniformly-charged "liquid drop" nuclei in nuclear physics are thus unified with the problem of equilibrium shapes and stability of ordinary liquid drops. Indeed, the object of liquid drop experiments at a scale directly accessible in the laboratory is to test not only the specific theory, but to provide markers in a much broader mapping of the properties of rotating fluid masses.

Confining discussion to the case of surface tension forces only (i.e., no self-gravitation, electrostatic interaction, or external gravitational field), it is necessary to define some of the parameters used to describe a free liquid drop in solid body rotation. The "free" drop is actually assumed to be contained within another fluid (for example, an atmosphere of gas) which rotates with the drop at the same angular velocity. The drop has density ρ_D and rotates with angular velocity Ω. The outer fluid has density $\rho_F < \rho_D$. The equilibrium shape of the drop must satisfy the equation[5]

$$\Delta P_o + \frac{1}{2} \Delta\rho \ \Omega^2 \ r_\perp^2 = \sigma \ \nabla\cdot\hat{n} \qquad (1)$$

subject to the constraint that the drop have a fixed volume. $\Delta P_o \equiv P_{Do} - P_{Fo}$ is the difference in pressures on the axis of rotation inside and outside the drop, $\Delta\rho = \rho_D - \rho_F$ is the density difference, $r_\perp$ is the radius perpendicular to the axis of rotation and extending to the drop's surface, σ is the interfacial tension, and $\hat{n}$ is the surface normal ($-1/2 \ \nabla\cdot\hat{n}$ is the local mean curvature).

If the density difference $\Delta\rho$ is zero, the effect of rotation (i.e., the centrifugal term $(1/2)\Delta\rho\Omega^2 r_\perp^2$) is completely removed and the shape satisfying Equation (1) would be a perfect sphere. Thus, no change of shape would result in the Plateau experiment if the whole tank were rotated. In this experiment, however, the drop was rotated differentially with respect to the outer fluid, giving rise to the analogous centrifugal term $(1/2)\rho(\Delta\Omega)^2 r_\perp^2$; this approach must suffer the effects of viscous drag and entrainment of the outer fluid. Some basis for comparison with the "free" drop system is preserved by making the outer fluid two orders of magnitude less viscous than the drop.

Returning to the free drop theory, Brown[5] rewrites Equation (1) in dimensionless form

$$Ha_o = K + 2\,\Sigma \left(\frac{r_\perp}{a_o}\right)^2 \tag{2}$$

where $H \equiv 1/2\nabla\cdot\hat{n}$ is the local mean curvature, a_o is the radius of a sphere having the same volume as the drop, and the parameters Σ and K are the rotational bond number† and dimensionless reference pressure defined by:

$$\Sigma \equiv \frac{\Omega^2 \Delta\rho a_o^{\,3}}{8\sigma} \tag{3}$$

$$K \equiv \frac{\Delta p_o a_o}{2\sigma} \tag{4}$$

Σ may also be considered as the square of a dimensionless angular velocity Ω', which for the neutral buoyancy experiment may be expressed as:

$$\Omega' \equiv \frac{\Omega}{\sqrt{\dfrac{8\sigma}{\Delta\rho a_o^{\,3}}}} \tag{3'}$$

†Chandrasekhar[6] uses a different definition of the rotational bond number:

$$\Sigma_{CH} \equiv \frac{\Omega^2}{\dfrac{8\sigma}{\Delta\rho a^3}}$$

where a is the equatorial radius of the axisymmetric rotating drop (as opposed to the resting radius a_o). This definition is convenient for the analytical treatment of axisymmetric figures of equilibrium, but the Σ used by Brown and in this paper is better for a generalization to non-axisymmetric shapes and as a basis for expressing experimental results. Note also that Σ_{CH} is identical to the parameter "e" used by Ross.[7]

Thus, the applicable equation for the neutral buoyancy tank is Equation (2) with $\Sigma = (\Omega')^2$.

Figure 2-1 shows cross-sectional profiles of axisymmetric shapes for values of Σ (from Wang[2a]). These cross-sections lie in a plane containing the axis of rotation (a meridianal plane). The figures which show a dip at the axis must not be confused with lobed shapes; they are biconcave discs similar in form to red blood cells. Figure 2-1 includes shapes which have broken completely away from the origin; the biconcave discs pinch off at $\Sigma = 1/2$ and become tori. ("Tori" is used loosely to describe all shapes which no longer intersect the Z axis.) Note that for a given Σ, i.e., an angular velocity, more than one axisymmetric figure can exist (see, for example, the two figures for $\Sigma = 1/2$).

The axisymmetric sequence excluding toroidal shapes may also be represented by a plot (Figure 2-2) of the dimensionless equatorial cross-sectional area against Σ.

Wang[2a] states that in the region $0 < \Sigma < 0.5$, there exist one simply-connected axisymmetric figure and one toroidal shape for each Σ; these families joint at $\Sigma = 0.5$ in a biconcave disc with zero thickness at its center. For Σ between 0.5 and 0.533, there are two toroidal and two simply-connected shapes. $\Sigma = 0.533$ is the maximum rotation rate for which a torus exists; its shape is unique. The two simply-connected shapes for each Σ continue to exist up to $\Sigma = \Sigma_{max} = 0.5685$; the shape at Σ_{max} is unique. Beyond Σ_{max}, there are no axisymmetric shapes possible for a free drop in rigid body rotation.

A substantial extension of the theory to include the shapes and stabilities of non-axisymmetric figures of equilibrium has been undertaken by Brown[5]. Along the simply-connected sequence the axisymmetric drop shape was shown to be stable to two-lobed perturbations for $\Sigma < 0.318 \equiv \Sigma_{II}$[6] (Brown calculates $\Sigma_{II} = 0.313$). At Σ_{II} the drop is neutrally stable to these perturbations and, above it, the axisymmetric shape becomes unstable. Similarly, Brown calculated bifurcation points to three- and four-lobed families from the simply connected sequence at $\Sigma_{III} = 0.5001$ and $\Sigma_{IV} = 0.5668$.[5] (See Figure 2-3).

Available data[2a,5,6,7a,10] on the calculated drop shapes have been collected in Appendix A. These data include the total energy, surface and kinetic energies, moment of inertia, and angular momentum, as well as area for each value of Σ.

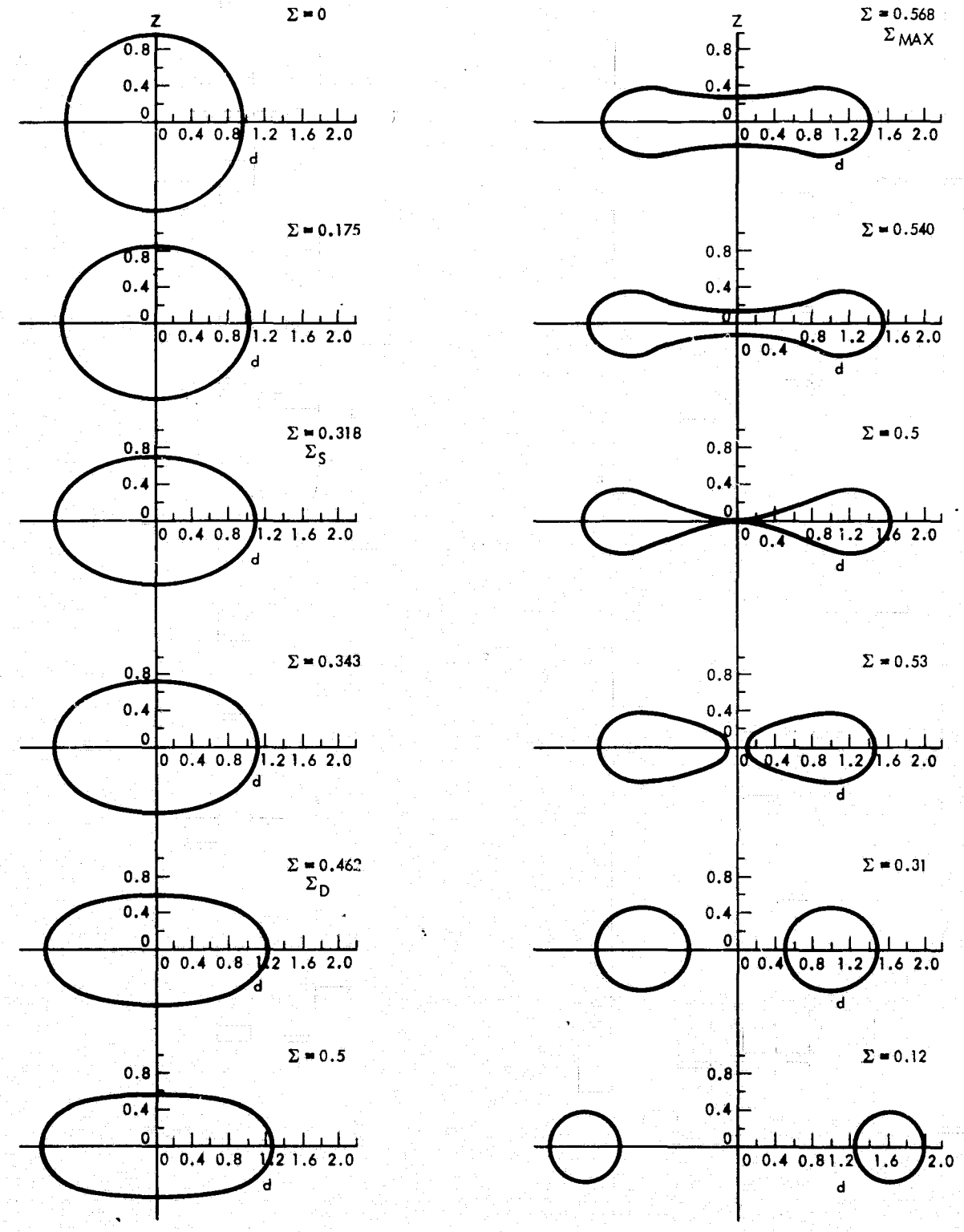

Figure 2-1. Axisymmetric Equilibrium Shapes[2a]

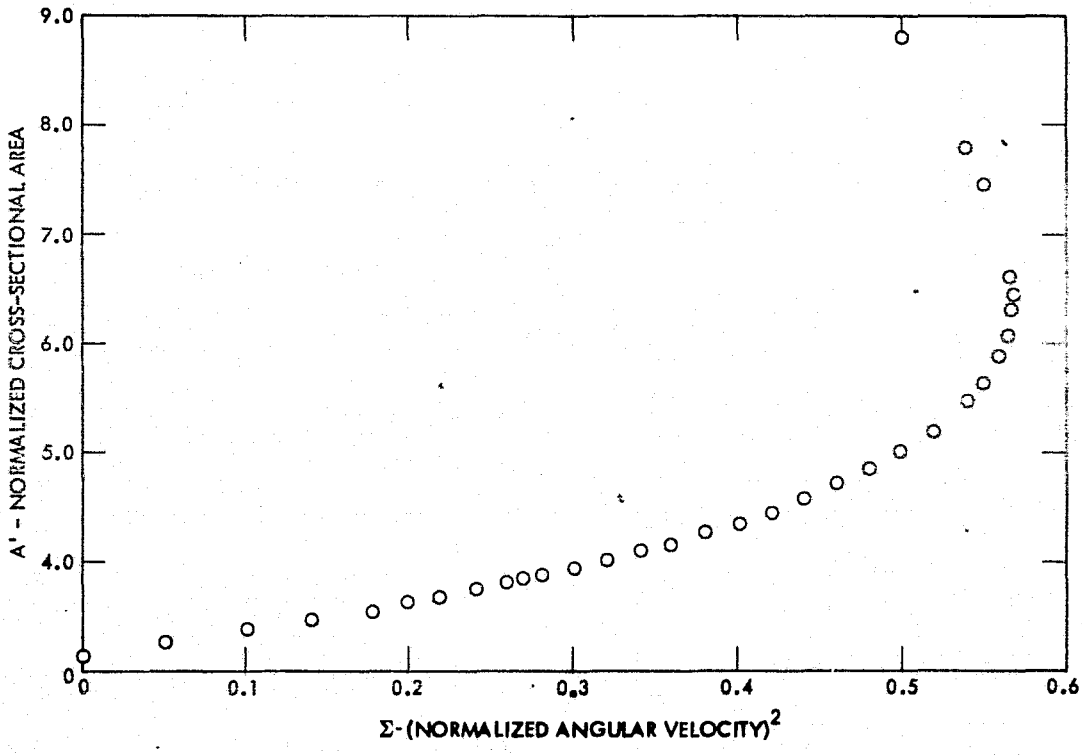

Figure 2-2. Calculated Equilibrium Shapes - Simply Connected Axisymmetric Shapes Only (i.e., up to pinch-off) (from Brown,[5] Chandrasekhar,[6] and Ross[7]).

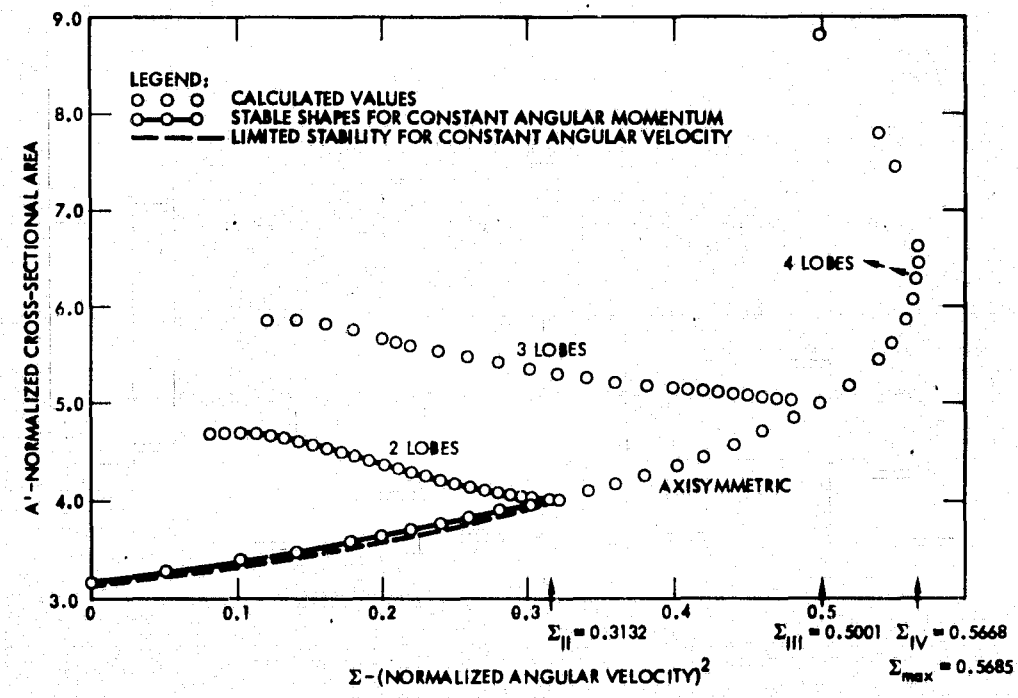

Figure 2-3. Calculated Equilibrium Shapes (from data given by Brown[5], supplemented by Chandrasekhar[6] and Ross[7]).

SECTION III

THE PREVIOUS EXPERIMENT

Plateau[1] has provided a richly detailed account of his observations of the neutral buoyancy experiment he devised; Figure 3-1 shows a sketch of his apparatus.

A brief summary of Plateau's observations is given here. He used an olive oil drop, 6 cm in diameter, centered around a 3.5 cm diameter disc and 1.5 mm diameter shaft, in an alcohol/water mixture.

At slow rotation rates (5 or 6 seconds per turn; $\Sigma \sim 0.02$), Plateau observed bulging at the equator and flattening of the poles; this behavior became more extreme as the rate increased; at roughly 2 to 3 revolutions per second, center thickness became negligible and the pellicle contracted into the major part of the drop to form a torus. Starting from a drop with 6 cm diameter, a ring of 10 cm would form and persist for roughly 10 seconds. Utilizing fluid from outside the drop as tracers, he found that the motion of the ring was that of a rigid body for several seconds. To prolong the length of observation, Plateau removed the disc and shaft when the ring formed and was able to study the collapse to a sphere. Most of Plateau's attention was focused on the tori which he thought were similar to the rings of Saturn. In the course of his observations, he studied other shapes (e.g., the two-lobed profile) which did not persist very long.

There are several other experimenters using density matching to study liquids in a gravity-freed environment. Carruthers and Grasso[12a,b] used this technique to study floating zones, the neutral buoyancy analog to the captive drop experiments, in which a drop is held between two cylinders which can rotate together or differentially. A sketch of their apparatus is shown in Figure 3-2.

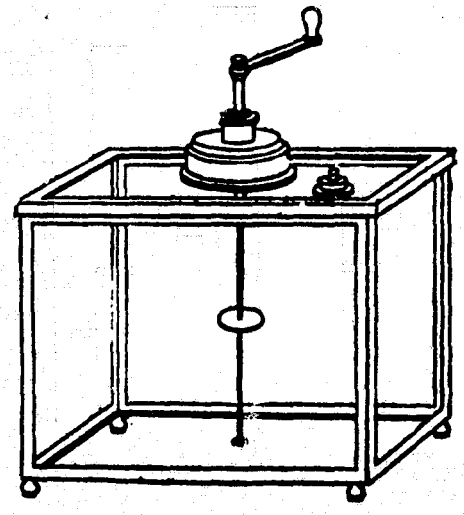

Figure 3-1. Plateau's Apparatus[1]

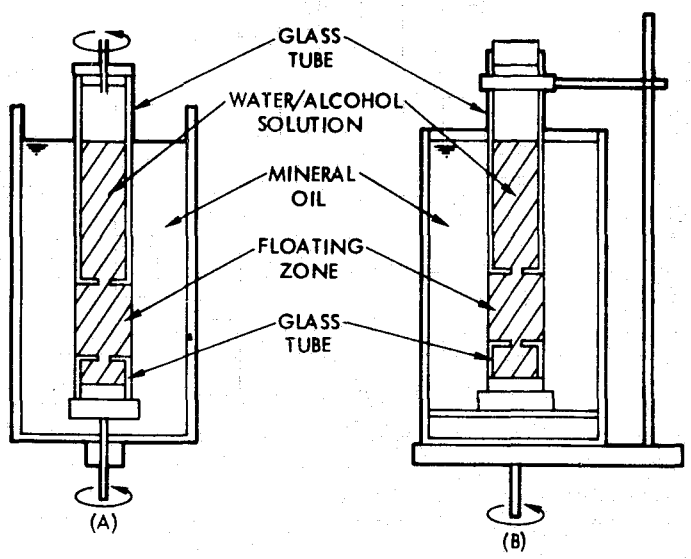

SCHEMATIC DRAWINGS OF EXPERIMENTAL APPARATUS FOR SIMULATING FLOATING LIQUID ZONES IN A ZERO GRAVITY ENVIRONMENT: (A) ROTATING GLASS SUPPORTING TUBES, (B) ROTATION OF WHOLE ASSEMBLY.

Figure 3-2. The Apparatus of Carruthers and Grasso[12b]

SECTION IV

JPL EXPERIMENT

A. THE APPARATUS

1. The Tank

The tank (see Figure 4-1) in which the drop is buoyantly supported and rotated consists of a Lucite cylinder† (height: ∿28.25 cm, diameter: ∿21.27 cm, wall thickness: ∿0.635 cm) which in turn is contained in a parallel-sided, cubical (27.9 x 27.9 x 27.9 cm) outer tank (wall thickness: 1.14 cm). Cylindrical symmetry about the axis of rotation is thus obtained while lens-like distortion of the drop inside the cylindrical tank is minimized by the parallel-sided geometry of the outer tank and the water circulating between it and the inner tank.

The circulating water is pumped into the system through 0.625 cm Tygon tubing from a constant-temperature bath (Labline Model 1246 with a Rota-set temperature regulator precise to 0.02°C) with a ∿15-liter capacity. A wire screen is placed in the line connected to the tank inlet to even the flow and to prevent the passage of air bubbles and foreign matter, which can interfere with the photography. The circulating water passes around and beneath the inner tank to provide a uniform temperature environment. Two O-rings set in a 1.27 cm thick Lucite spacing plate separate the inner tank, outer tank, and the surroundings from each other with airtight seals. Prior to running the experiment, the tank components are cleaned with soap and water and rinsed with distilled water; organic solvents (especially acetone) are never used in order to avoid etching the Lucite.

2. The Shaft and Bearings

The present design of the shaft is shown in Figure 4-2. The shaft and disc are turned from a 2.54 cm diameter stainless steel rod with extreme caution to maintain straightness. The shaft, once placed in the tank, wobbles near the disc less than 0.16 mm. The part of the shaft in contact with the drop has been made as thin as possible to minimize distortion of the resting drop from the spherical shape it would have if it were floating freely. The critical dimensions of the shaft governing the experimental results are the radius of the disc (1.232 cm) and the radius of the narrow part of the shaft (0.081 cm). This is a volume of roughly 0.5 cm^3; typical drop volumes are about 12 cm^3. Other dimensions are used in calibrating the photographs taken during the experimental runs.

---

†The Lucite cylinder was obtained from Cadillac Plastics, Inc., 11255 Vanowen St., North Hollywood, Ca. 91605

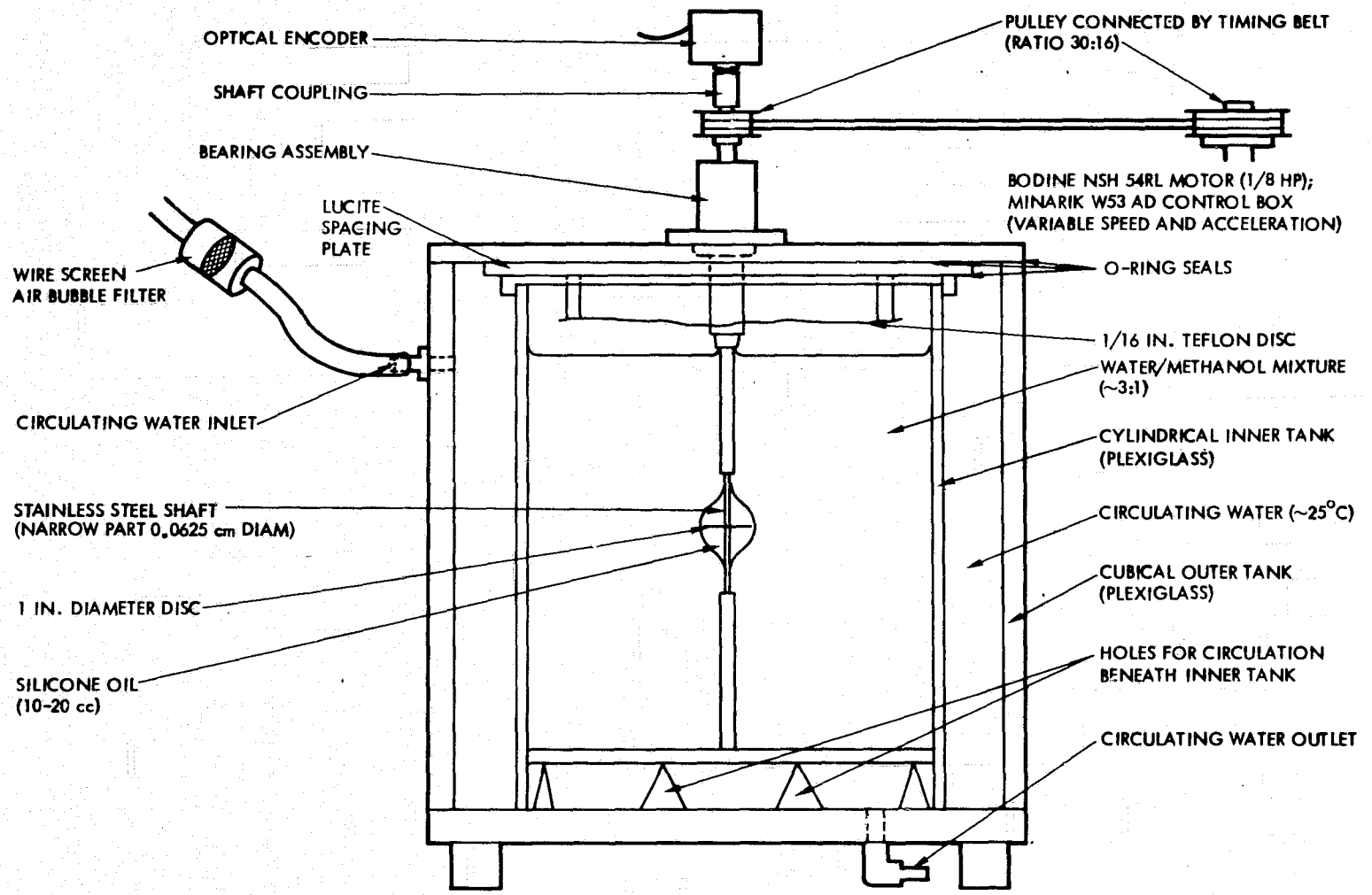

Figure 4-1. Immiscible System Apparatus

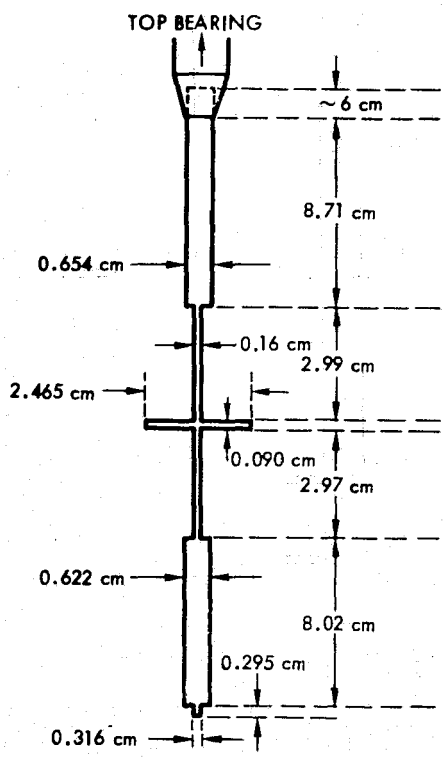

Figure 4-2. Shaft Dimensions

The lower bearing is simply a hole bored partly through the bottom of the inner tank. The bottom of the shaft has a narrow stub which fits into the hole with a 0.0625 cm gap between the end of the stub and the bottom of the hole. This space allows some vertical play when positioning the shaft into the inner tank so the shaft will not bow due to insufficient spacing between the bearings. The hole and stub diameters have a close tolerance to prevent lateral motion of the shaft and yet still allow smooth rotation without binding.

The upper bearing is a cylindrical bearing with ball races; the inner cylinder of the bearing is bored out and tapered at its lower end so that the shaft slips inside about 0.635 cm. The shaft has recently been held snugly in this bearing with stainless-steel shims instead of set-screws. The upper bearing is held in a flanged brass housing which is screwed down to the Lucite lid of the tank.

Coupled to the upper end of the shaft is a Rotaswitch optical encoder, Model 881-1000-OBLP-TTL which puts out 1000 5-volt pulses per revolution of the shaft. This output is used to generate a numerical display of the shaft rotation rate.

3. Motor and Pulleys

The motor used to drive the shaft is a Bodine NSH 54RL motor rated at 1/8 hp; it is coupled to the shaft with pulleys in a 30:16 ratio (motor:shaft). The belt and pulleys have mating notches to prevent slipping. The motor is mounted on an upright of the wooden frame which is used to support the tank above bench level to facilitate photography. A Minarik W53 AD control box allowing variable acceleration up to a variable final speed and variable decelerations to rest is used to control the motor.

4. Electronics

To assist with analysis of the motion picture films taken of the experiment, digital seven-segment LED displays have been constructed to provide the following information: time (from 0.01 s to 99.99 s); a number representing the period of rotation of the shaft; date; and film and "run" numbers. The date, film, and run numbers (the last distinguishes different spin up sequences on the same film) are set by BCD thumbwheel switches. All of the displays are recorded on film (see below) and thus, each frame of film has several numbers to identify it.

In addition to the digital displays, a plot of the shaft velocity is generated while running the experiment. The pulses from the encoder are also sent to a digital/analog converter which produces a voltage proportional to the pulse rate. This voltage is tied to the Y-channel of a Hewlett-Packard Model 7034A plotter set to sweep the X-axis uniformly in time. While the pulse rate converter/plotter arrangement is not believed to give an accurate representation of the acceleration and deceleration of the shaft because of response-time problems, the steady maximum speeds are plotted well enough for qualitative real-time comparisons of different trials or "runs" of the experiment.

B. THE FLUIDS

The rotating drops are formed from Dow Corning 200 Fluid silicone oil and range in volume from 10 to 18 cc. This fluid is a polydimethylsiloxane available with viscosities ranging from 0.65 centistoke to 100,000 centistokes. Most of the work was done using the 100 centistoke fluid because this viscosity is two orders of magnitude higher than that of the surrounding fluid but still low enough to be away from the critically damped region. The density of the 100 centistoke oil at 25°C is 0.963 g/ml. Samples of various oil-soluble dyes were obtained*; DuPont "Oil Bronze" dye when mixed with the silicone oil was found to provide good photographic contrast between the drop and the background. The supporting liquid was a mixture of water and methanol in proportions

*DuPont Organic Dye and Keystone Dyes (Keystone Dye is supplied from Ingham Corp., Cerritos, Calif. 90701).

initially found by trial and error to match the density of the silicone oil at the operating temperature. 100 centistoke oil required roughly a 3 to 1 water/methanol mixture at 25°C. The physical properties, such as density and viscosity at various temperatures, of water and methanol mixtures of given compositions are well documented.[13] Based on this published data, Figure 4-3 shows how the density of such mixtures can be matched with the density of the silicone oil*. The viscosity of the density-matching mixture (taken as 22 percent methanol by weight) is 1.5 centistokes at 25°C[13e]. Temperature is a very critical factor, and hence, the need for precise control (±0.2°C) of the temperature of the system.

The drop is prepared by stirring roughly 0.35 grams of dye into a 200 milliliter sample of silicone oil and allowing it to dissolve for several hours. This mixture makes the drop sufficiently dark to be

*An eventual improvement in the choice of drop and supporting fluids would be to match their indices of refraction as well as their densities to eliminate optical distortions of the positions of trace particles inside the drop (see below regarding flow visualization). Also, thus far, no effort has been made to specially purify the working fluids.

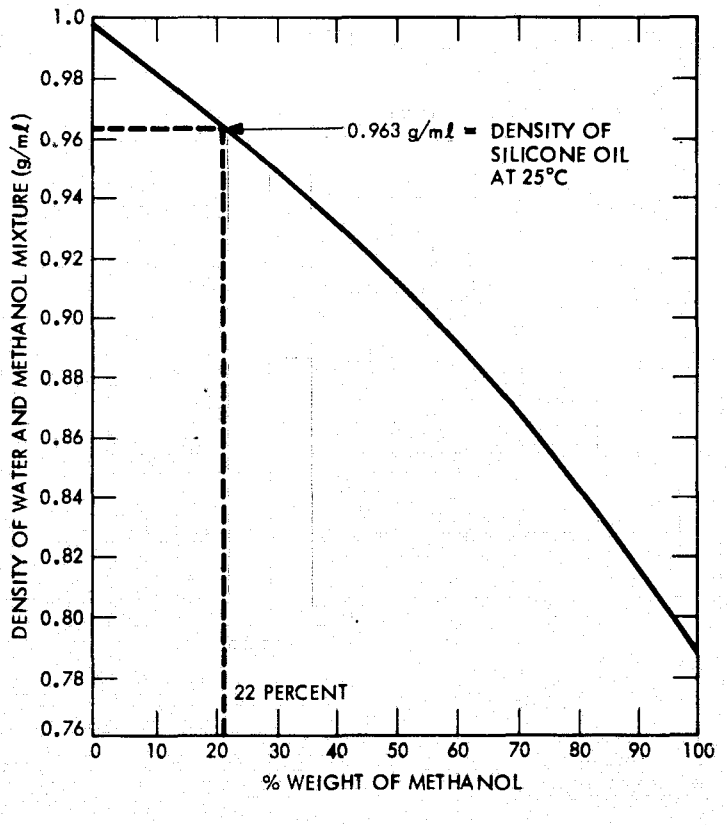

Figure 4-3. Matching the Density of Silicone Oil and the Water/Methanol Mixture at 25°C; the Solid Line shows the Variation of Mixture Density with Composition (from Carr and Riddick[13e])

distinguishable against a bright background but still transparent enough for particles inside the drop to be seen. It has been found necessary to strain the dyed oil through coarse filter paper to remove undissolved particles of dye. The water and methanol mixture is prepared in roughly the right proportions in large glass bottles. The dye will cause variation of the oil density, and hence, uncertainty in the proportions. About 8 liters of mixture are poured into the inner cylinder of the experimental tank; the outer tank is then filled with distilled water pumped in from the constant-temperature bath. In this process air bubbles form and attach themselves to the cylinder wall and the base; they must be removed.

Prior to this point, the shaft has been inserted into the upper bearing. The narrow portion of the shaft is coated with a thin layer of silicone stopcock grease using a small brush; the disc (top and bottom) is coated with some of the dyed silicone oil using a syringe. The purpose of coating the shaft prior to immersing into the water/methanol mixture is to ensure uniform wetting of the shaft by the silicone oil and hence, proper centering of the drop around the shaft. An uncoated shaft, after exposure to the water and methanol mixture or to air for a prolonged time, will eventually be wetted poorly by the silicone oil, and inconsistent results will be obtained when spinning the drop. The most consistent results are obtained for a 0° contact angle between the oil and the shaft (See Figure 4-4). The coated shaft is placed into the tank through the large hole in the lid, the bottom of the shaft is slipped into the lower bearing, and then the upper bearing

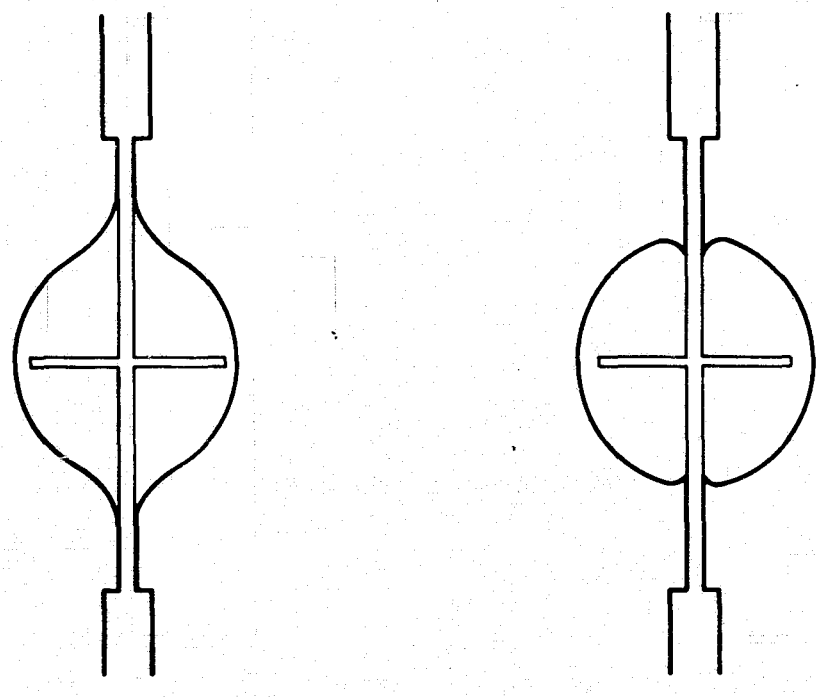

Figure 4-4. Good and Poor Wetting of the Shaft by the Silicone Oil

is screwed down to the lid. The O-ring in the flange on the upper bearing provides an airtight seal around the large hole. A rubber stopper is placed in the small "manipulating port" in the lid to completely seal off the inner tank. With the temperature regulator, circulating pump, and fluorescent lamps all on, the system is allowed to equilibrate overnight.

Once the system has been brought to equilibrium at the operating temperature (preferably so the center of the inner tank is 25 ±0.2C°.), test drops of the dyed silicone oil are injected into the water/methanol mixture using a syringe with a long stainless steel tube; 1 to 2 millimeter diameter droplets are formed at the end of the tube and shaken loose. Air bubbles must be avoided. If the test drop rises to the surface of the mixture, more methanol must be added. If the test drop falls, more water is needed. The exact stable position of the test drop will depend on the density gradient of the tank. The origin and exact character of this density gradient is presently under investigation; the gradient has been found to be on the order of 5×10^{-4} g/cc/cm. This was done by measuring the densities and vertical positions of test drops of three slightly different densities (Figure 4-5 a and b; also Figure 1-1); the slight density differences were obtained by mixing different viscosity grades of silicone oil and dyeing the mixtures different colors. The positions of the drops were measured with a cathetometer; the densities were later determined by observing the volume of each oil sample in a precision-volume flask on an analytical balance. This density gradient may be due to inhomogeneities in the mixture, or to the temperature gradient.

The temperature gradient (Figure 4-6) was found by measuring temperatures at various heights within the tank using a Veco 51A1 Thermistor Probe sealed with RTV to the end of a long glass tube. (The probe had previously been calibrated against a precision (0.01°C) mercury thermometer in the constant temperature bath.) The sharp rise in temperature near the surface is probably due to heat introduced by the fluorescent lamp resting on the top of the tank. (Note: since the tank is airtight, there should be no evaporation from the free surface of the water and methanol mixture.)

The interfacial tension must be determined between the oil and surrounding water/methanol mixture. Unfortunately, methods for determining interfacial tensions[16] (e.g., the Wilhelmy plate[14] and pendant drop[15] methods shown in Figure 4-7) require density differences between the two fluids. Thus, the approach of Carruthers and Grasso[12] is taken; the interfacial tension is measured for water/methanol mixtures with density not equal to the silicone oil density and a plot of interfacial tension versus concentration of methanol is obtained. Interpolation then yields the interfacial tension for the density-matching concentration. This work is still in progress, and the final results will be published separately[17]. Extrapolation of measurements done thus far, as shown in Figure 4-8, using the pendant drop method to measure interfacial tension between undyed silicone oil and the water/methanol mixture yields a value of 28 ±1.5 dynes/cm for a methanol concentration of

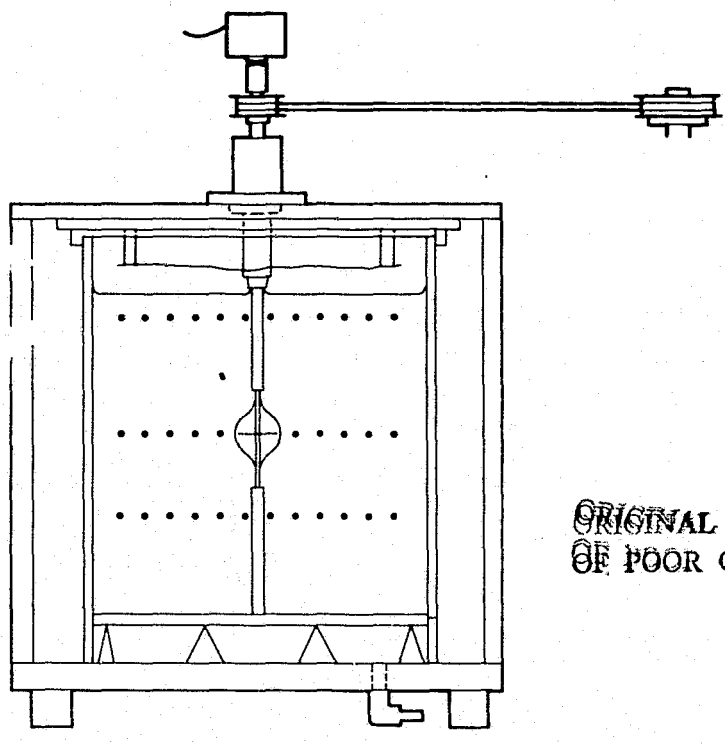

Figure 4-5a. Estimating the Density Gradient in the Neutral Buoyancy System Using Three Different Densities of Silicone Oil to Form Planes of Test Drops

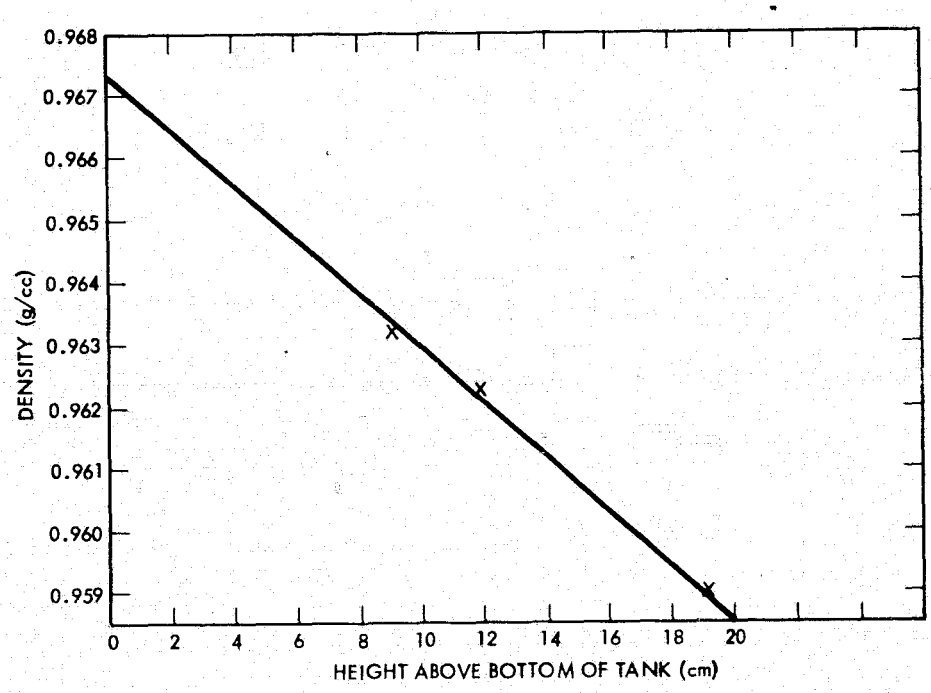

Figure 4-5b. Density Versus Height Measurements [A linear fit to the three points gives a density gradient of 4.4×10^{-4}(g/cc)/cm].

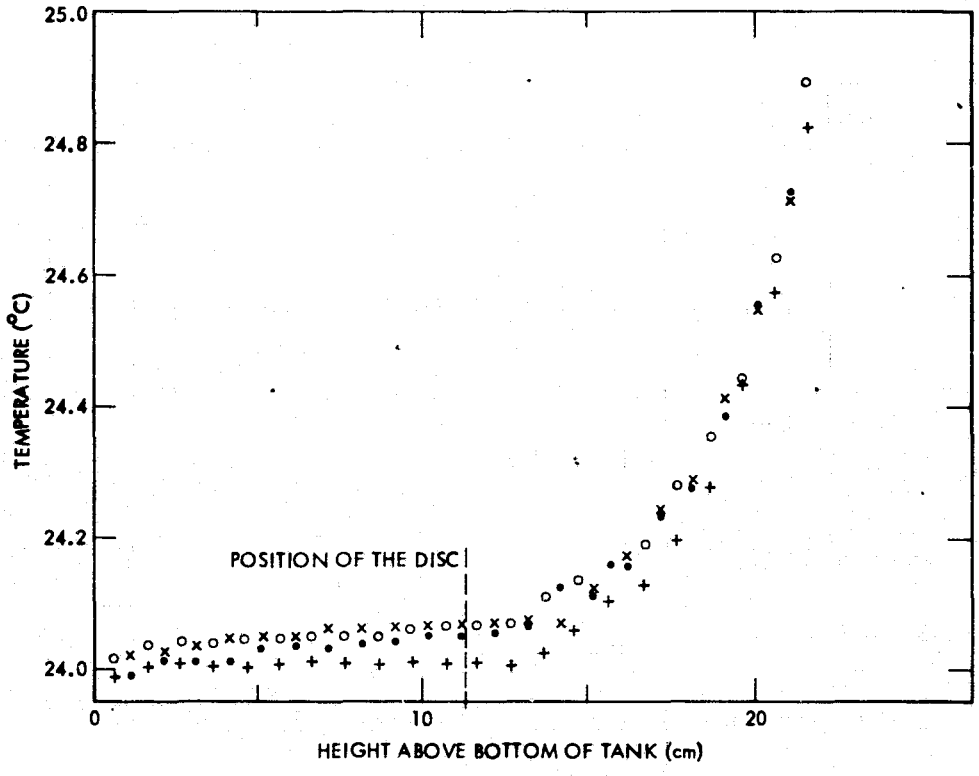

Figure 4-6. Temperature Profile of the Neutral Buoyancy Tank (Measurements made by Tom Chuh)

22 percent, by weight, the density matching concentration. The validity of making a linear extrapolation must still be checked. The rotating bubble method[18] may eventually be used to check and extend the present measurements.

C. PHOTOGRAPHY

1. Mirror Optics

By using the system of three mirrors shown in Figure 4-9, virtual images of two orthogonal views (e.g., front and bottom) of an object in the tank can be formed in the same plane*. The experiment set-up is shown in Figure 4-10. Examples of the resulting photographs, giving a bottom view and front view of the shaft and drop along with the digital displays, are shown in Figures 5-1 through 5-12.

---

*An ingenious system for combining three orthogonal views and digital displays was recently designed by Fred Chamberlain at JPL.

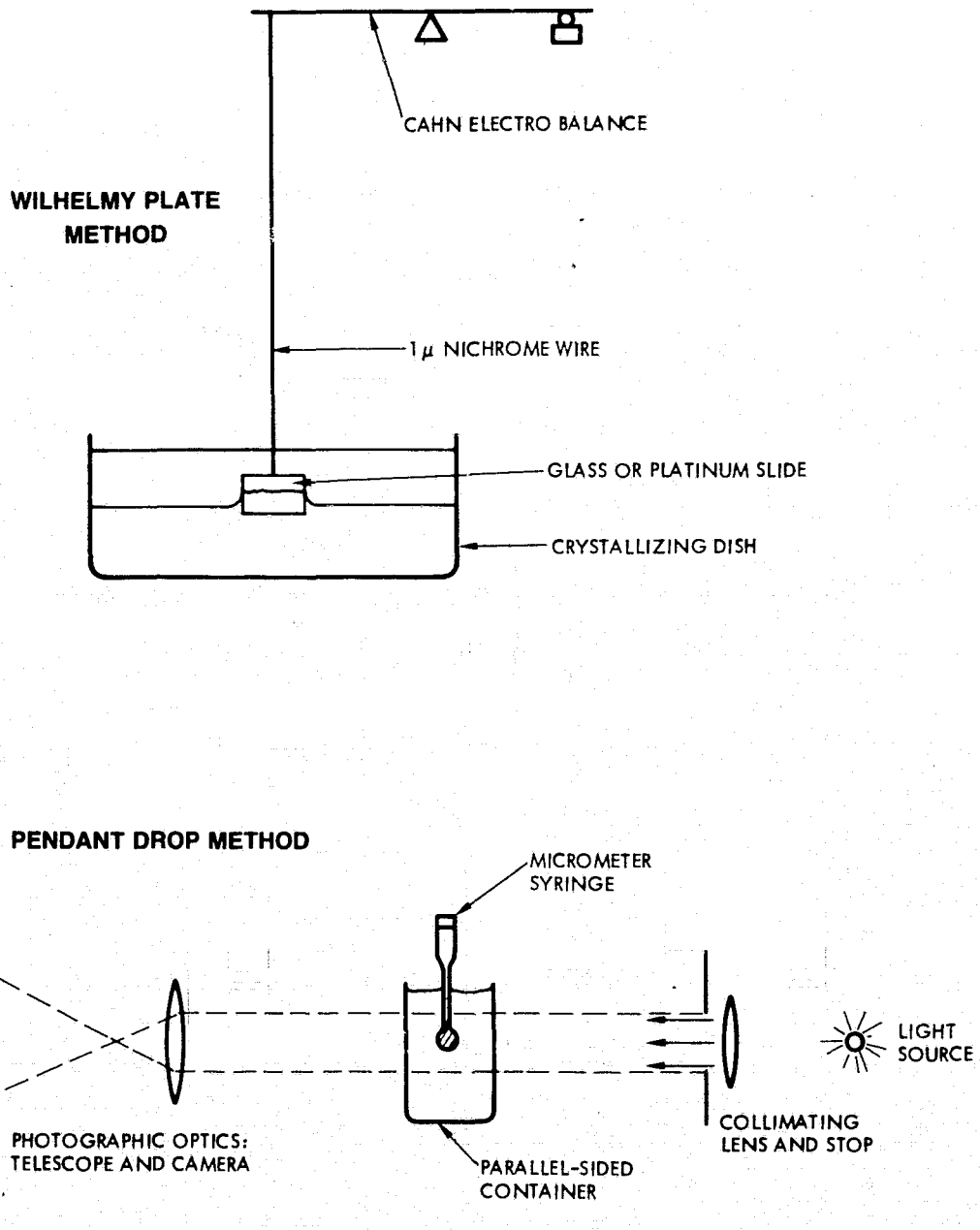

Figure 4-7. Methods for Measuring Interfacial Tensions

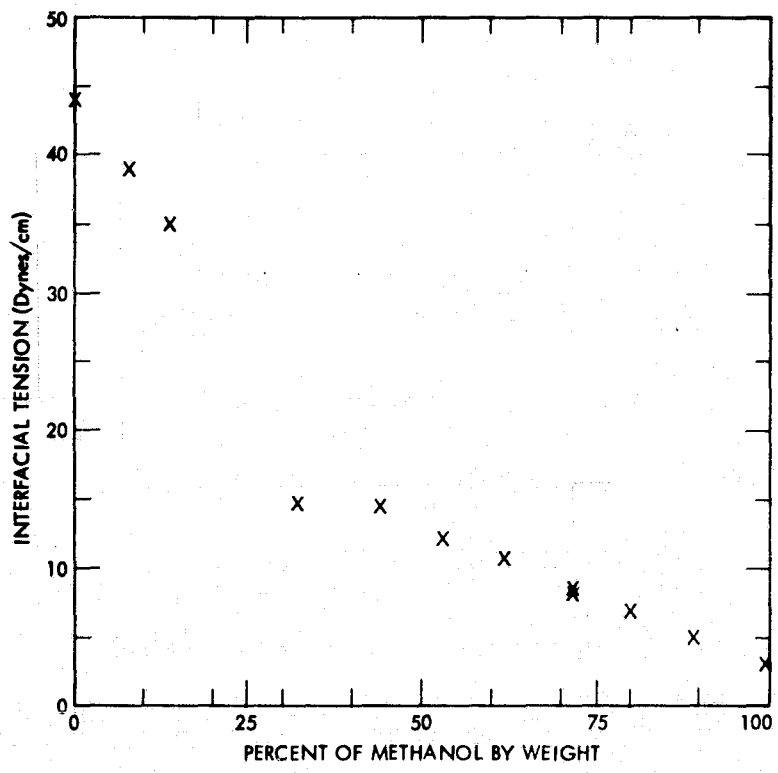

Figure 4-8. Interfacial Surface Tension Between Silicone Oil and a Mixture of Water and Methanol (using pendant drop method)

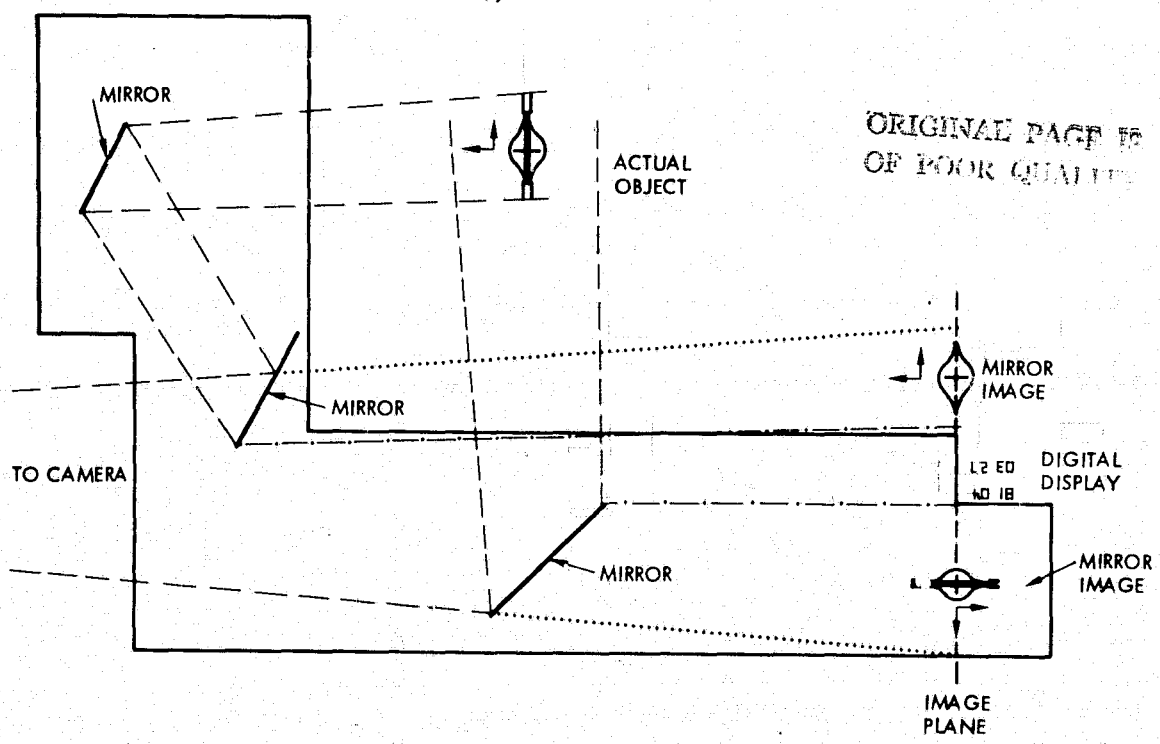

Figure 4-9. Optics which Incorporate Two Orthogonal Views and a Display onto a Single Frame of Film

2. Lighting

After a review of the literature on drop and bubble photography[19], the method of diffuse backlighting was chosen. Circular fluorescent lamps (Sylvania "Circline" 22 watt "Rapid Start" lamps) as shown in Figures 4-10 and 1-1, are positioned about 3.81 cm from diffusing sheets of Teflon or opal glass. The diffusing materials give broad, evenly bright backgrounds. Against such a background, the perimeter of the drop stands out quite clearly. Hyzer[19] and others noted that, because the drop has a specularly reflecting surface, an erroneous image of the drop perimeter is produced when diffusely scattered light is used instead of a collimated beam. However, the camera in this experiment was placed far enough away from the object (1.4 meters) to make this effect negligible. The fluorescent lamps produce incorrect color rendition on the film, but this posed no problem in the analyses.

3. Film

Kodak Ektachrome 7242 EF 16 mm motion picture film (with high-speed perforations) was used to record the behavior of the rotating drops. This is a color film with an ASA rating of 125, suitable for indoor use under Tungsten lighting.

4. Cameras and Lenses

Initially, a spring-wound Bolex H-16 camera was used at its maximum speed of 64 frames per second. The Bolex was replaced with a Milliken DBM-55 camera fitted with reflex viewing which could operate at speeds from 0 to 400 frames per second. About 2 seconds were

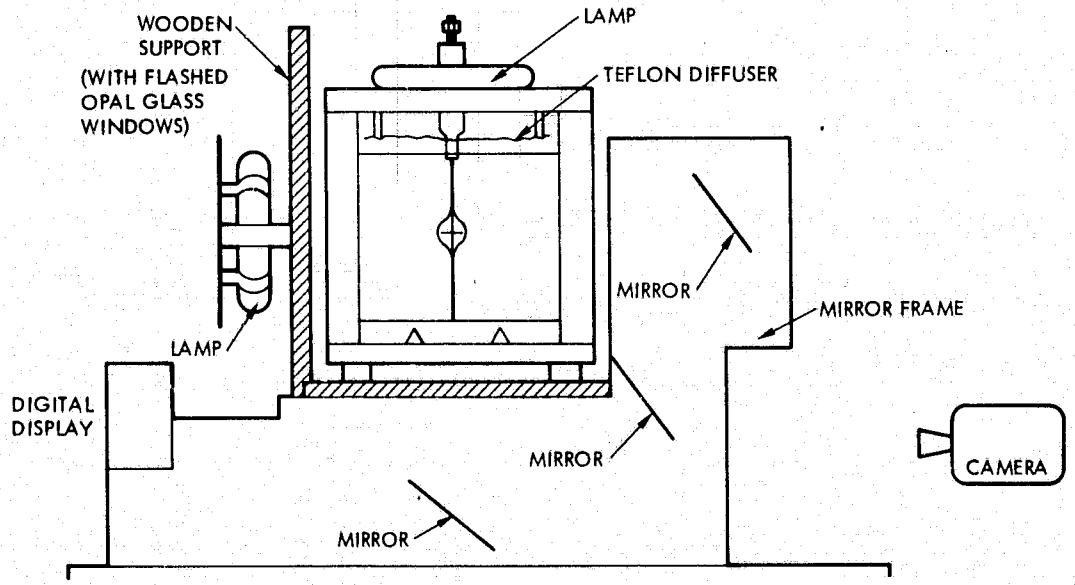

Figure 4-10. Experimental Setup During Data Acquisition

required for the camera to come up to speed. The lens used was made by Schneider with a focal length of 50 mm opened up to f/2.8 at a shooting distance of 1.43 meters and a film speed of 50 frames per second.

D. FLOW VISUALIZATION

1. Inside the Drop

Flow visualization inside the drop is crucial for quantitative investigations. The drop rotates at a significantly different speed from that of the shaft; a measure of the shaft speed is thus not sufficient for comparison to theory. The drop is not in uniform solid-body rotation due to the shear close to the disc. Velocity profiles (e.g., angular velocity versus radial distance from the shaft) must be measured.

The internal flow visualization is accomplished by forming trace particles out of the water/methanol mixture. A 20 cc sample of the mixture is withdrawn from the tank using a syringe. The sample is ejected into a beaker and dyed until virtually opaque. The sample is always removed from a level higher than that of the disc so that when its density is increased by the addition of the dye, the final density better matches that of the silicone oil. The level from which the sample is withdrawn is found by trial and error. The trace drops are formed by injecting small (0.5 to 1.0 mm diameter) droplets of the dyed mixture into the silicone oil drop. About 20 droplets are injected. If the droplets are too small, they will be hard to follow from frame to frame when analyzing the film. Large droplets, on the other hand, may significantly alter the rotating drop behavior. Thus far, no perturbations caused by the tracer drops have been observed.

2. The Supporting Fluid

Flow visualization in the outer fluid provides a measure of the transfer of angular momentum with time from the shaft and drop to the supporting mixture. The drop behavior of particular interest is that which occurs after "spin-up" of the drop but before the angular momentum carried by the outer fluid becomes a sizeable fraction of that of the drop. Studies of the external flow have so far been limited. Hollow glass beads (Eccospheres) and aluminum flakes have been used under dark field illumination (i.e., against a dark background with only light scattered from an intense source reaching the camera) with limited success; density matching and visibility of individual tracers from frame to frame are difficult problems. At present, no satisfactory approach has been developed.

E. RUNNING THE EXPERIMENT

The experiment is run after the following have been performed:

(1) The densities are matched at the desired temperature (usually 25°C) and the buoyancy level brought to within 1 cm of the disc

(2) The drop is in place and symmetric around the shaft (radially) and about the disc (vertically)

(3) The camera and mirrors are aligned and ready; digital displays, pulse rate converter, and plotter are on

(4) Tracers have been injected into the drop.

Beyond this point, care is taken to avoid altering the volume of the drop. Constant volume from run to run is desirable to allow direct comparison, but is not absolutely necessary since separate volume measurements are to be made from the stationary drop profiles prior to each run. At high speeds, fission of the drop is unavoidable and even though most of the oil can be collected and reinserted into the main drop, small amounts of oil are usually lost. Also, manipulations of the drop with the syringe and stainless tube (e.g., to inject more tracers or to position the drop) can cause slight volume changes.

The experiment is run in the following manner:

(1) The velocity, acceleration, and deceleration dials on the motor control are chosen.

(2) The clock is reset, simultaneously starting the sweep on the x,y plotter.

(3) The camera is switched on and allowed to come to a steady speed (about 2 seconds).

(4) The motor switch is turned on, the drop rotated for 10 to 30 seconds, and the motor turned off.

(5) The drop motion is allowed to die out; then the camera is stopped.

Prior to the next run, the motor direction is reversed, the drop is re-centered and tracers redistributed if necessary using short fast spins, and the system is allowed to settle for at least 5 minutes until no motion of the outer fluid is perceptible. (The test drops of silicone oil are left freely floating as motion indicators in addition to showing the position of the buoyancy level.) Each run is carried out with the motor spinning in the opposite direciton from that of the previous run.

SECTION V

QUALITATIVE RESULTS

A record of the distinct shapes that have been observed is shown in Figures 5-1 through 5-12. These shapes are:

(a) Figure 5-1. Drop At Rest

(b) Figure 5-2. Axisymmetric Oblate

(c) Figure 5-3. Axisymmetric Biconcave

(d) Figure 5-4. Two-Lobe

(e) Figure 5-5. Three-Lobe

(f) Figure 5-6. Four-Lobe

(g) Figure 5-7. Torus

(h) Figure 5-8. Torus Pinching Off

(i) Figure 5-9. Torus Completely Broken Up

(j) Figure 5-10. Single Lobe (Ultimate Decay Shape)

(k) Figure 5-11. Sessile Two-Lobe (A Decay Mode)

(l) Figure 5-12. Tilted Two-Lobe (A Decay Mode)

The five basic families of shapes are axisymmetric, two-lobed, three-lobed, four-lobed, and toroidal. Additionally, the off-axis single lobe is the final shape for all experimental runs except those in which the drop undergoes fracture. This shape is thought to be an artifact of the apparatus, a consequence of slight initial asymmetries, and of inconstant adhesion by the drop to the shaft.

Examples of the basic shapes have been found to develop and persist for several seconds before decaying to lower modes and/or finally to the asymmetric single lobe. Figures 5-13 to 5-17 show sequences of development and decay for each of these families. Runs in which such clearly defined behavior fails to occur often result when the drop is poorly centered at the outset, or there is too much residual motion of the surrounding fluid.

Apart from the axisymmetric shapes at slow rotation rates, the three-lobed family was the easiest to obtain. This fact was due in part to the particular drop volumes and shaft dimensions used in this experiment. The ease with which three-lobed shapes are generated is nevertheless remarkable; even in an early, very crude 1/4-scale version of the experiment, three-lobed shapes were readily obtained.

Two-lobed shapes, which develop for slower shaft velocities (<2 rps), may be harder to obtain because the decay processes which cause the drop to form into an asymmetric single lobe may set in before the drop can develop symmetric lobes. Four-lobed shapes, on the other hand, are obtained at generally higher shaft velocities ($\sim$4 rps) than the three-lobed shapes; when asymmetries develop in the drop at these angular velocities, fracture usually results.

During the decay of higher non-axisymmetric modes, one-lobe generally rotates faster than the others, eventually catching up and joining with the lobe preceding it. Thus three converge into two and two into one. This is not surprising; the mass of the drop is never equally distributed among the lobes; so one lobe is smaller and suffers less drag by the surrounding fluid. The presence of drag is immediately apparent from the pinwheel appearance of all of the lobed shapes, with the lobes curving backwards against the direction of rotation.

A further effect, attributed to the motion of the outer fluid, appears in many runs in which two- and three-lobed shapes are produced; in the course of the drop's development, the drop rises and becomes sessile on top of the disc (i.e., it only contacts the upper surface of the disc and shaft). Three-lobes decay to two-lobes which are sessile (Figure 5-11) and often persist for many seconds before decaying to a single lobe (also sessile). This rising of the drop occurs even when the level of exact density matching is below the disc by, for example, two centimeters. Furthermore, above a rather well-defined shaft velocity midway in the range of velocities producing three-lobed shapes, a different effect occurs. The three-lobed drop still decays to a two-lobed one but with one lobe above the disc and the other below, i.e., the drop is tilted (Figure 5-12).* This appears to be a very stable geometry which can persist for a minute or more.

Only a few instances of the toroidal shape have been observed with this system. This is probably because the drops used were of much smaller volume relative to the shaft dimensions than in Plateau's investigations[1] (15cc as opposed to 100cc). Nevertheless, striking examples have been photographed of the formation of a torus and its subsequent highly symmetric fracture into three or four large drops and a corresponding number of small satellite drops (Figures 5-7 through 5-9 and Figure 5-17).

The question of whether or not shapes with five or more lobes can be obtained is unresolved. Brown's calculations[5] show the four-lobe family as the last one branching off the axisymmetric sequence for the case of a free drop. Nevertheless, early trials with more viscous drops (1000 centistokes instead of 100 centistokes) seemed to indicate the posibility of producing more lobes. However, there is no photographic record, and the lobes may not have been as clearly formed as first perceived.

---

*In our analysis, the two-lobed shapes resulting from decay of higher modes have not been considered to be representative of the two-lobed family. Too much momentum has been transferred by this point to the outer fluid.

The sequence {axisymmetric → two-lobed → three-lobed → four-lobed} seems to be linked to increasing shaft angular velocity. It is less certain where the toroidal shapes arise. If the drop, upon spinning up, proceeds roughly through a series of axisymmetric equilibrium shapes before forming lobes, the progression is understood by comparison to Figure 2-5 for the free drop: The two-, three-, and four-lobed branch points are at progressively higher values of Σ, and hence, of angular velocity. It is expected that the lobed shape must rotate more slowly than the axisymmetric shape seen just before lobe formation. Although a higher spin-up velocity is required for higher lobes, the fully developed lobed shapes probably do not differ greatly in their angular velocities.

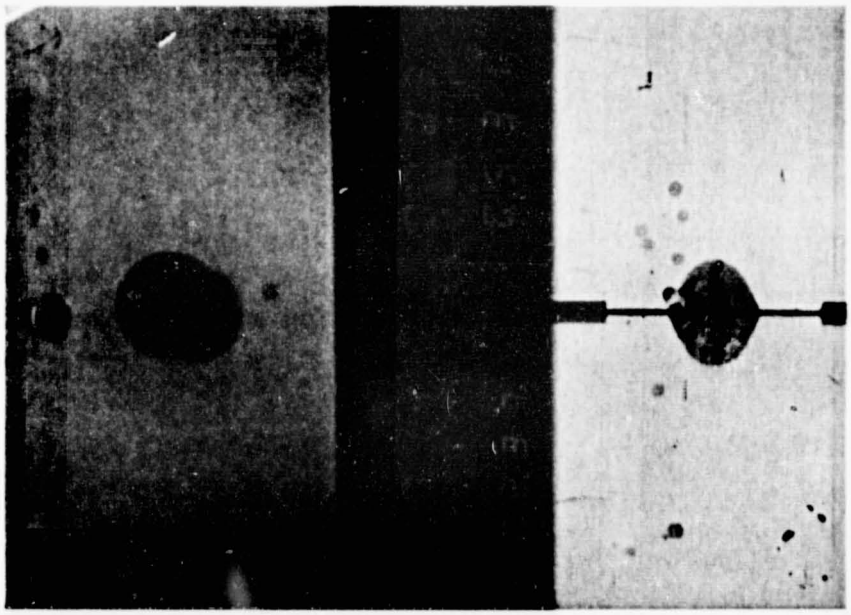

Figure 5-2. Axisymmetric Oblate Drop. (Shaft angular velocity = 0.8 rps)

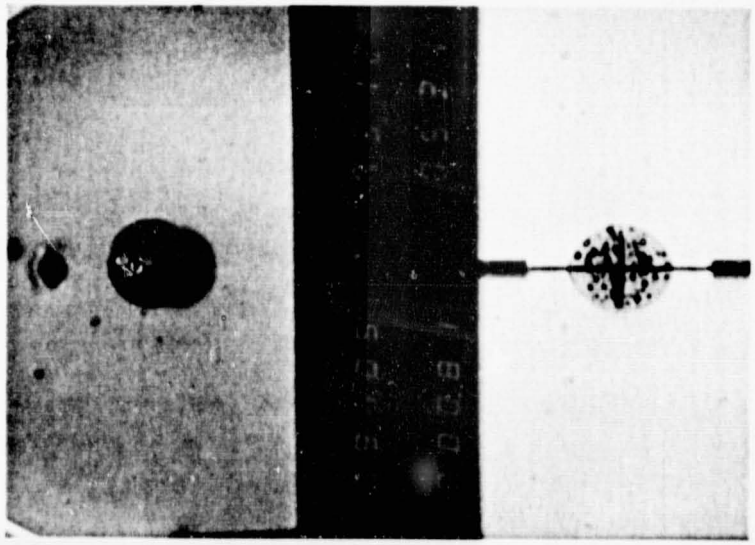

Figure 5-1. Drop At Rest. Note internal trace drops and external satellite drops

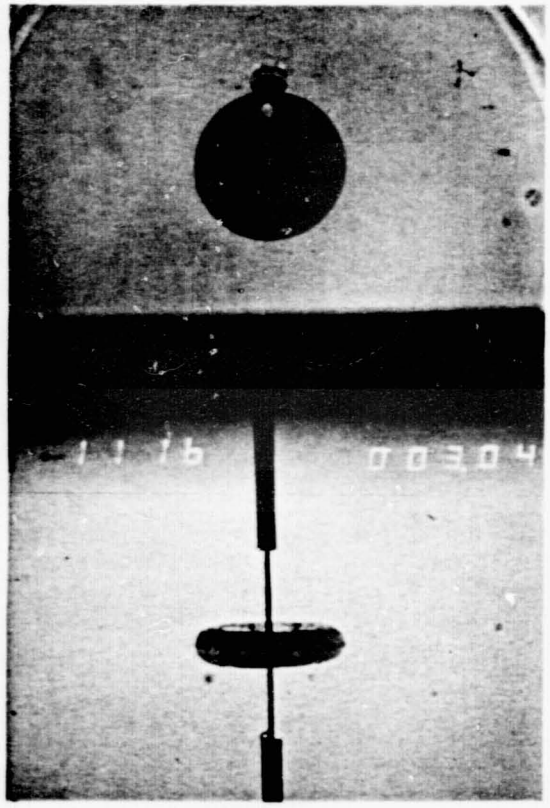

Figure 5-3. Axisymmetric Biconcave Drop (Shaft angular velocity = 1.8 rps); drop is still spinning up)

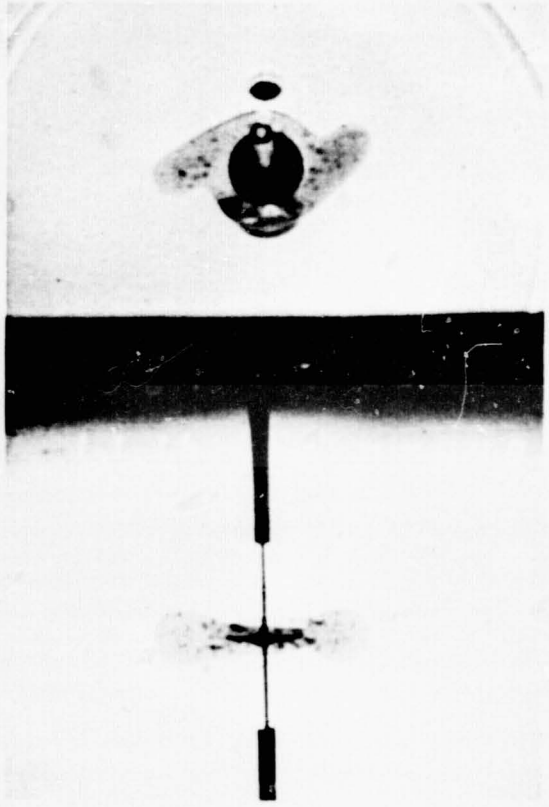

Figure 5-4. Two-Lobed Shape (Shaft angular velocity = 1.8 rps)

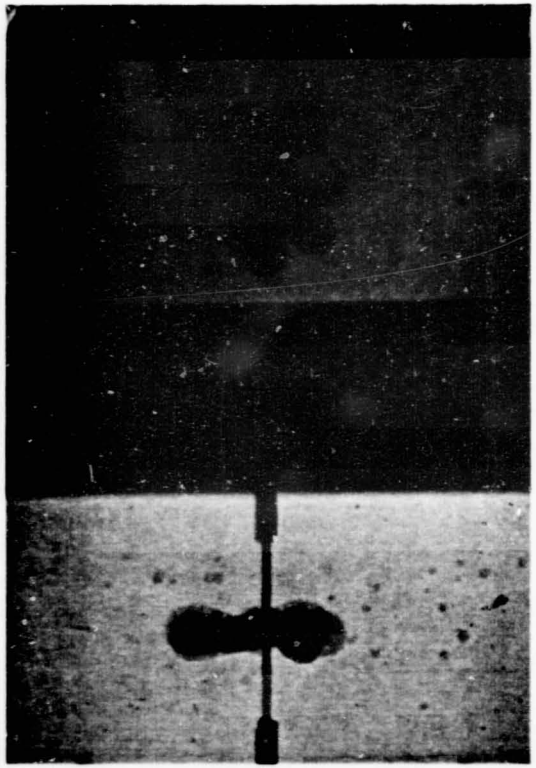

Figure 5-5. Three-Lobed Shape (Shaft angular velocity = 2.0 rps)

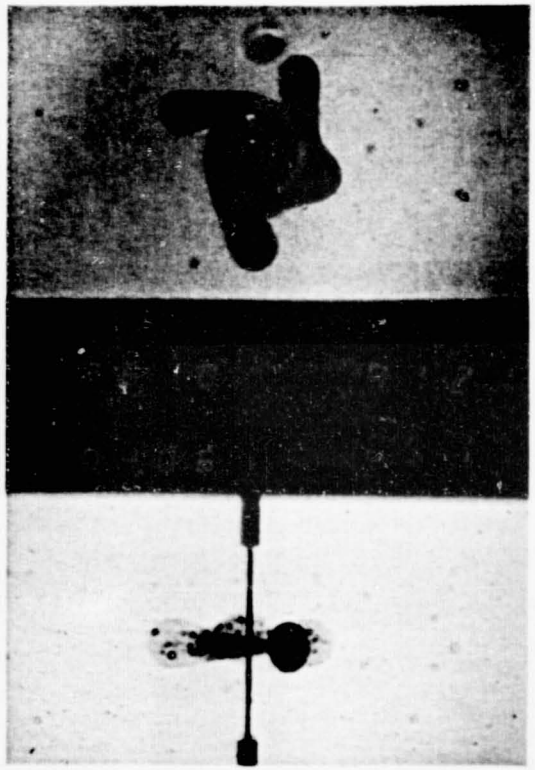

Figure 5-6. Four-Lobed Shape (Shaft angular velocity = 3.8 rps)

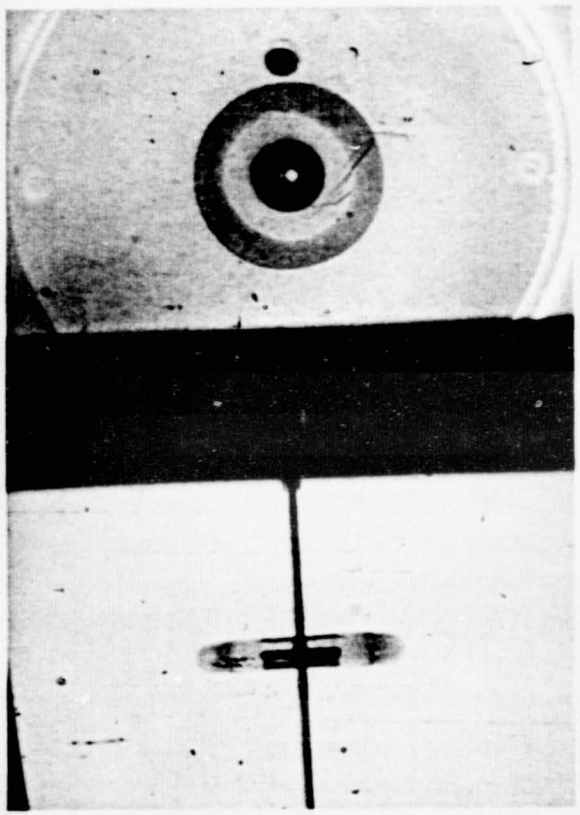

Figure 5-7. Torus (Shaft angular velocity = 4.8 rps)

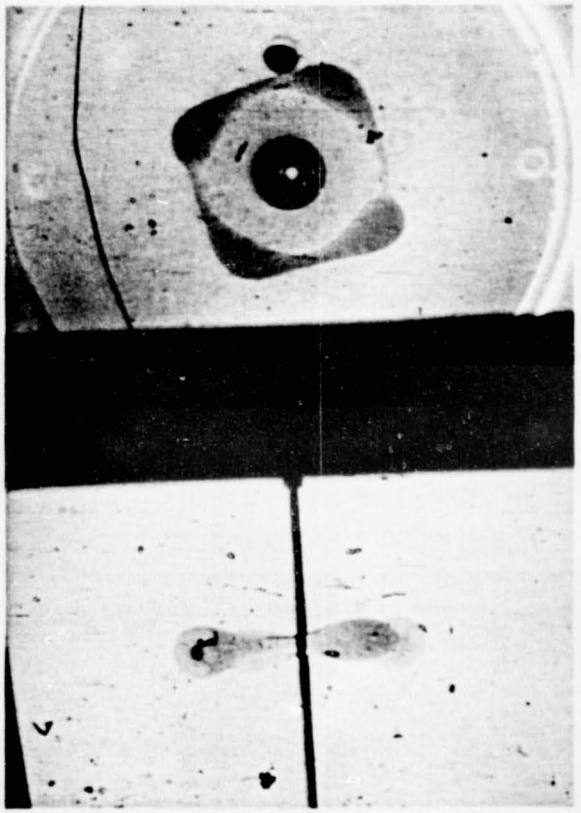

Figure 5-8. Torus Pinching Off (Shaft is not rotating)

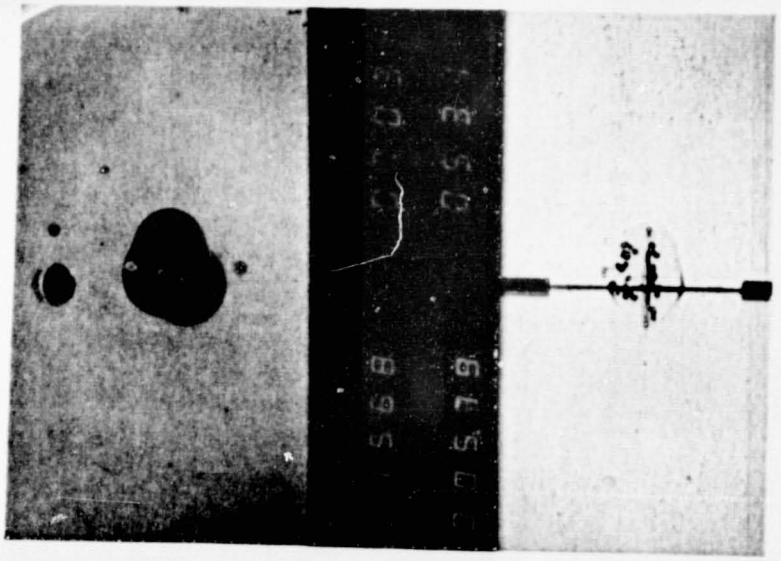

Figure 5-10. Single Lobe (Ultimate decay shape)

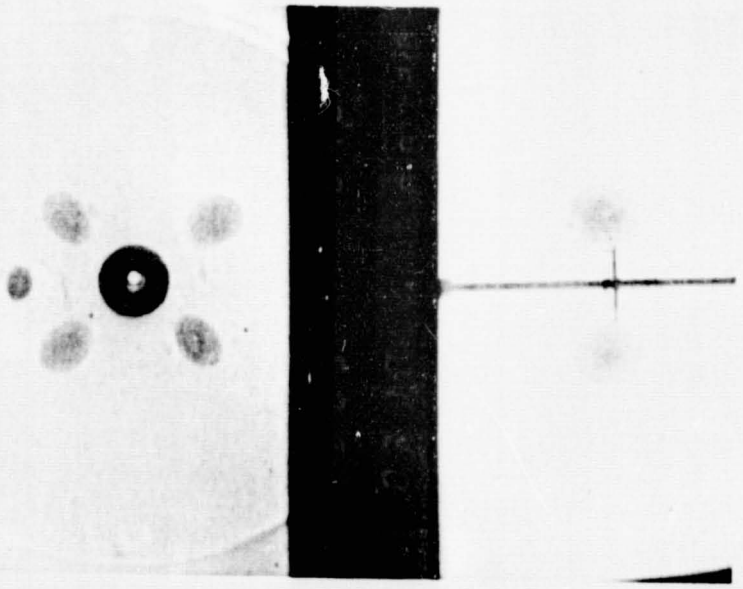

Figure 5-9. Torus Completely Broken Up (Shaft is not rotating)

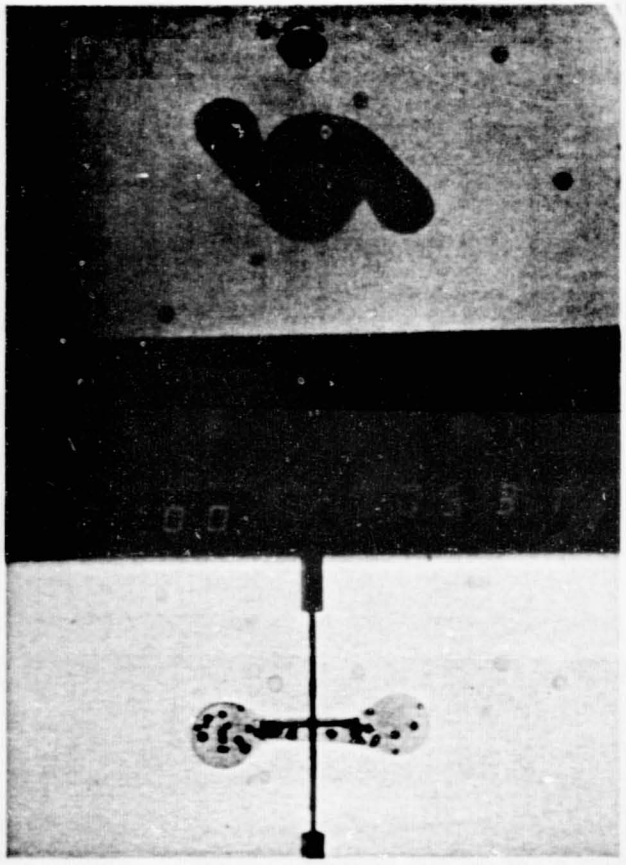

Figure 5-11. Sessile Two-Lobed Shape (The results of decay from a three-lobed shape; shaft is not rotating)

Figure 5-12. Tilted Two-Lobed Shape (Decay route for three-lobed shapes)

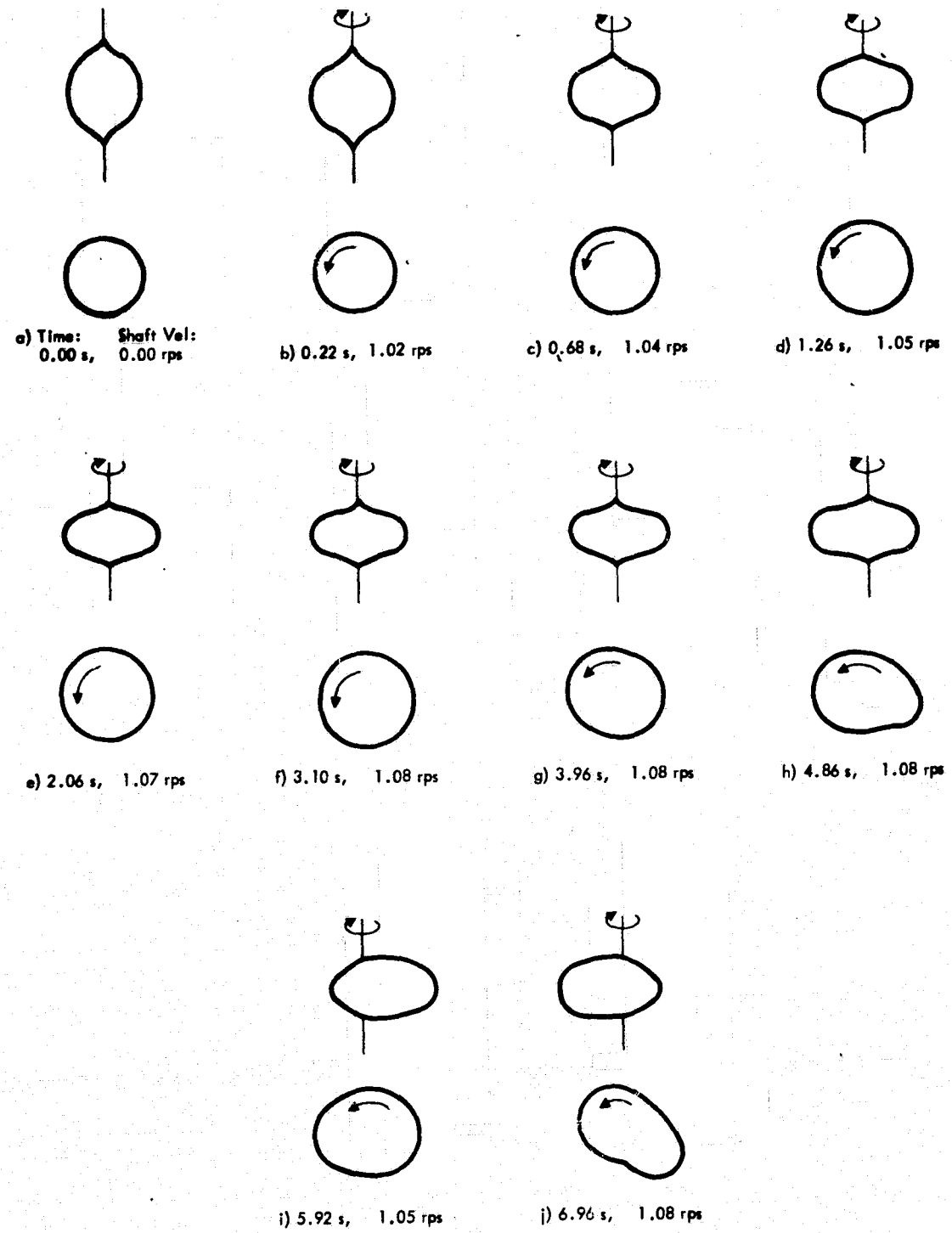

Figure 5-13. Example of an Axisymmetric Run (Film 107-110, Run 4) a) Stationary drop; b&c) Spin up; d-f) Axisymmetric; g) Beginning of loss of axial symmetry; h-j) Decay to single lobe. Each panel shows time elapsed in the run and the angular velocity of the shaft.

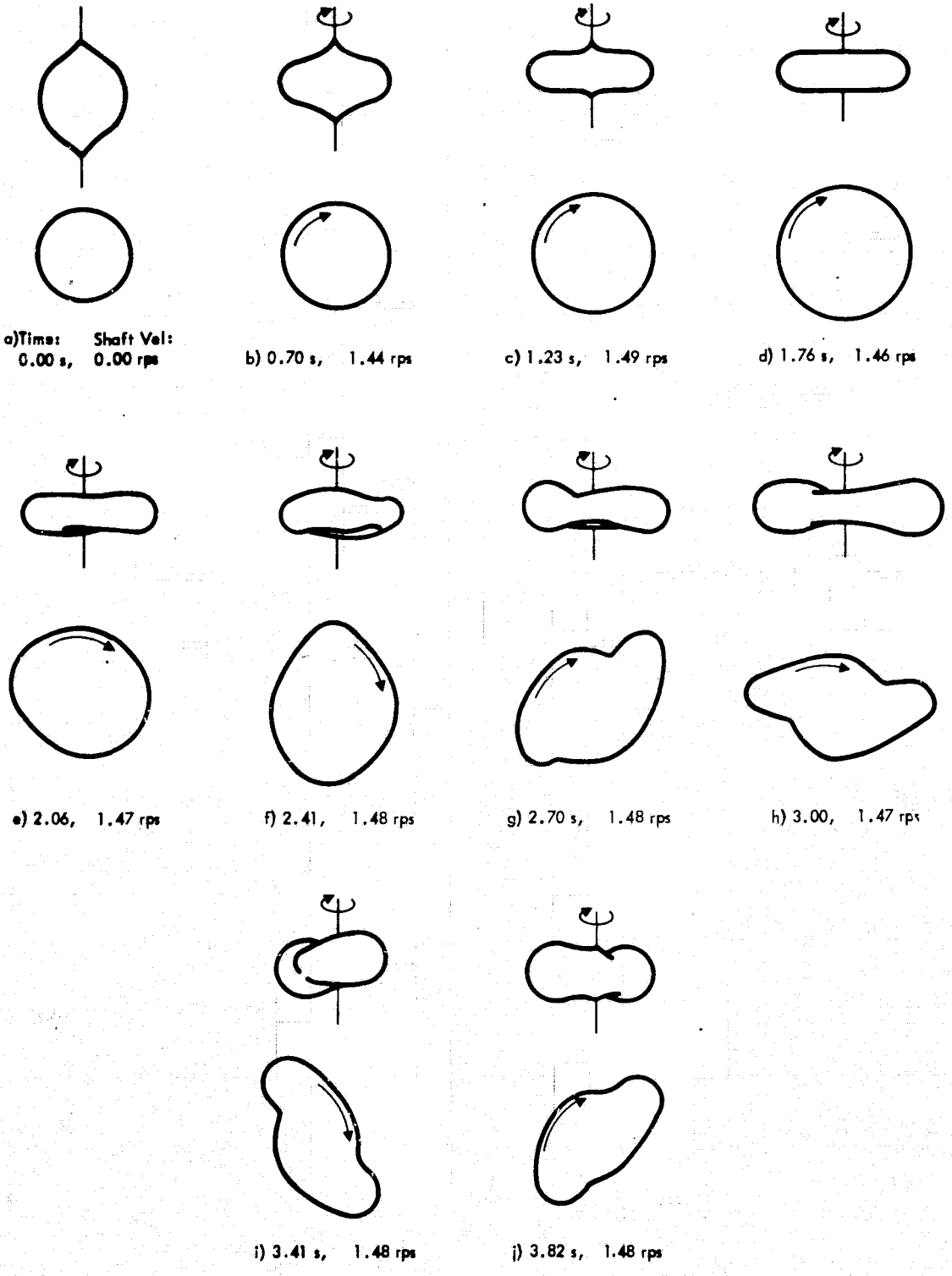

Figure 5-14. Example of a Two Lobe Run (Film 99-102, Run 8) a) Stationary drop; (b&c) Spin up; d) Axisymmetric; e) Initial loss of axial symmetry; f) Development of 2-lobed shape; g-i) Fully developed 2-lobed shape; j) Beginning of decay to one lobe.

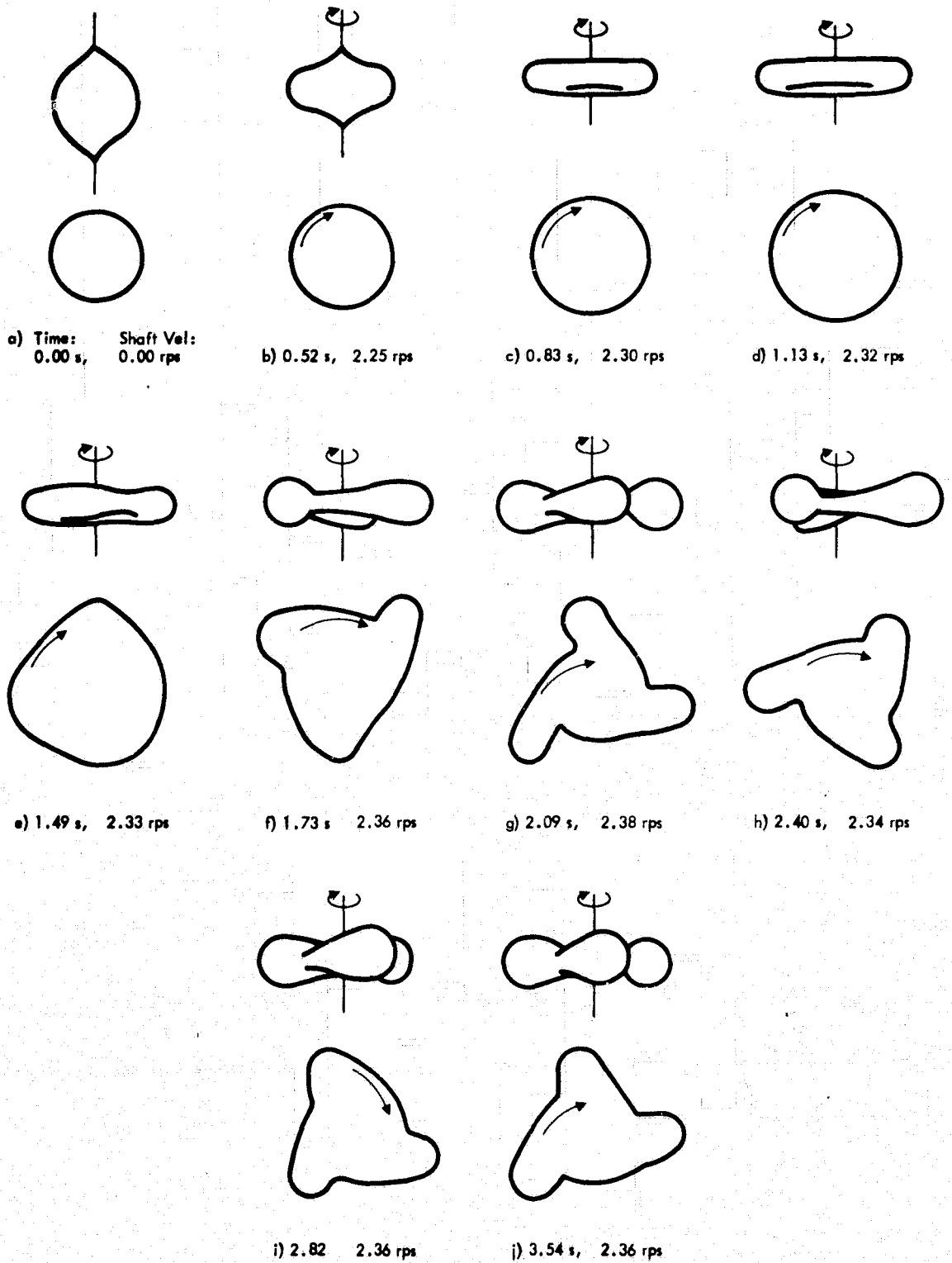

Figure 5-15. Example of a Three Lobe Run (Film 103-106, Run 13)
a) Stationary drop; b) Spin up; c) Biconcave, axisymmetric; d) Loss of axial symmetry; e&f) Development of 3-lobed shape; g-i) 3-lobed shape; j) Beginning of decay to two lobes.

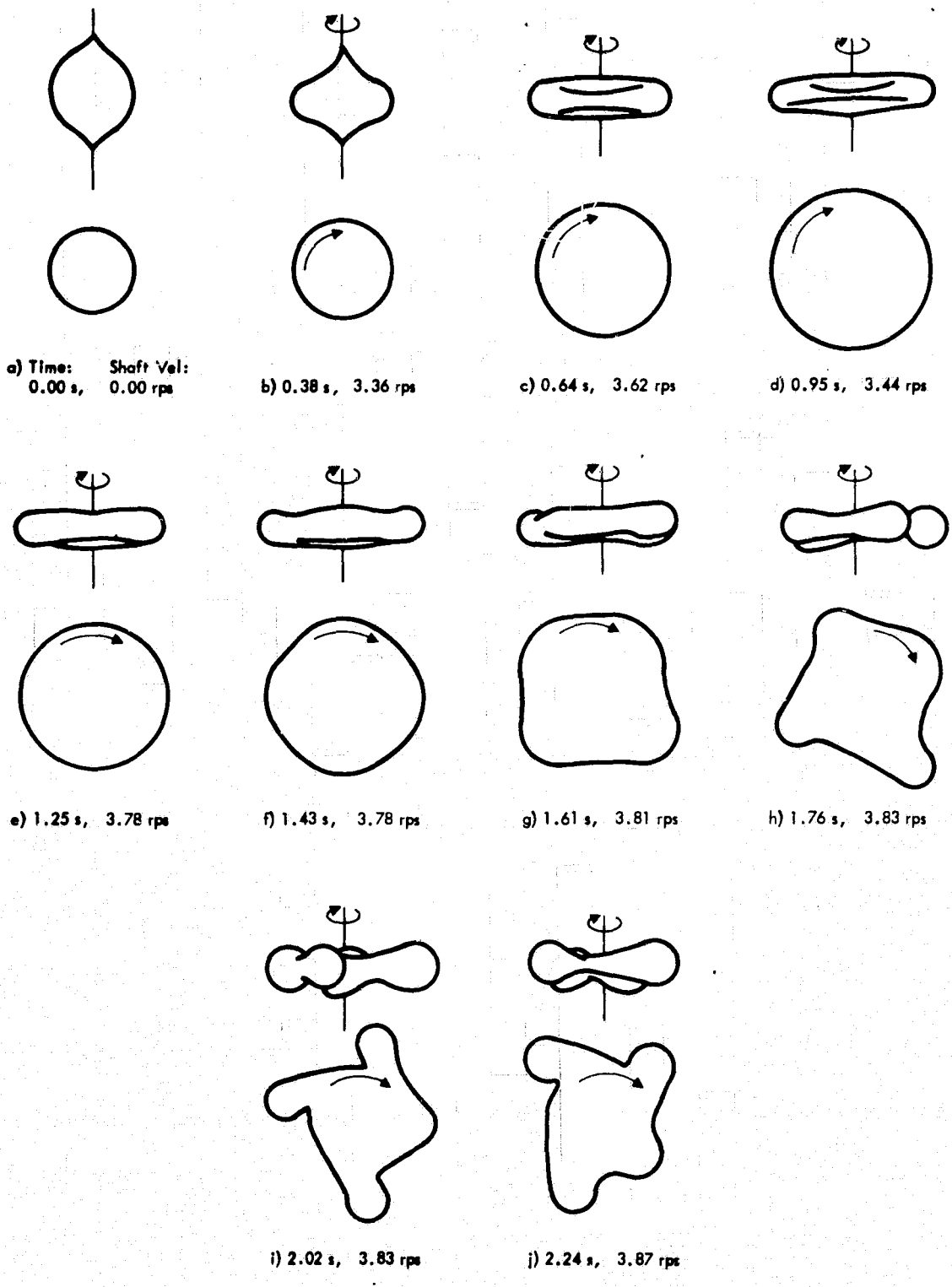

Figure 5-16. Example of a Four Lobe Run (Film 91-94, Run 21)
a) Stationary drop; b) Spin up; c) Biconcave, axisymmetric; d) End of axial symmetry; e-g) Development of 4 lobes; h&i) Definite 4-lobed shape; j) Beginning of decay to three lobes.

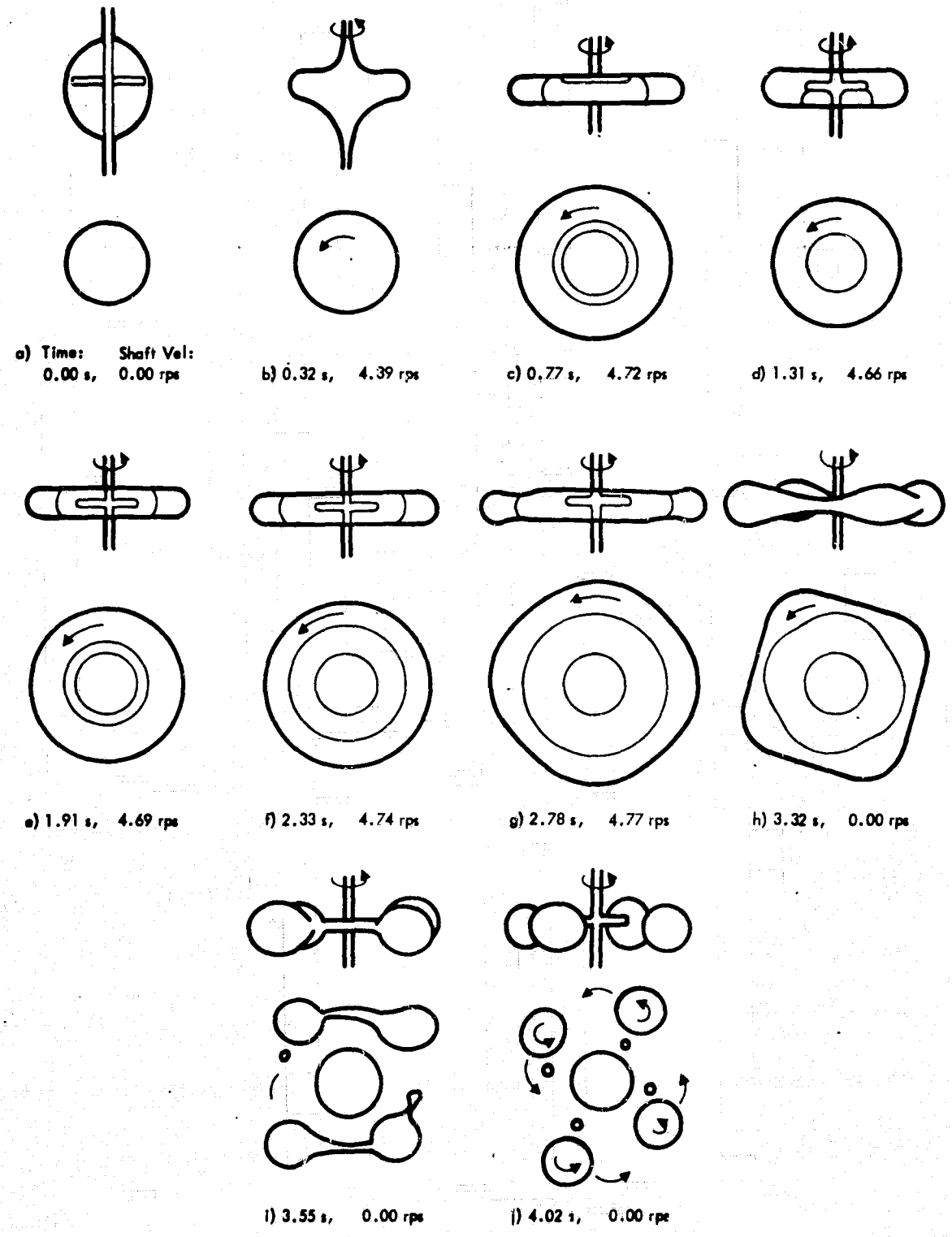

Figure 5-17. Example of a Toroidal Run (Film 43, Run 3) a) Stationary drop; b) Spin up; c) Axisymmetric, tenuous connection to disc; d) Rebound; e) Initial toroidal shape; f) Torus; g) Loss of axial symmetry; h) Four corner torus; i) Pinch off; j) Final fracture to four large and four small spheres.

SECTION VI

FILM ANALYSIS SYSTEM

In the course of these investigations, over 2000 feet of 16 mm film have been produced suitable for quantitative analysis, with additional footage devoted to earlier qualitative studies. The task of data extraction from photographic images is formidable; using motion pictures compounds the problem. Each of our films consists of a series of experimental runs lasting in real time from 10 to 30 seconds; since a high-speed camera is used, time is expended on playback of the film. A run consists of spin-up, development, and decay of a rotating drop. Each frame of film contains a record of date, film number, run number and a clock reading (Figure 6-1); all resulting data is correspondingly identified. Only certain runs have been selected for analysis using the following criteria: clarity of the drop profiles, symmetry of the drop profiles, and clarity and dispersion of the trace droplets. Thus far, the numbers of runs analyzed in the manner described below are:

(a) Axisymmetric: 12

(b) Two-lobed: 2

(c) Three-lobed: 2

(d) Four-lobed: 1

A run is characterized by the type of shape which occurs just before decay or fracture.

From a time sequence of two-dimensional images, the behavior of a three-dimensional system is to be inferred. The heart of the analysis procedure is the ability to reliably measure XY coordinates on the image. Devices of many levels of sophistication for this purpose exist on the market today; an older model Vanguard Motion Analyzer with a 16 mm projection head was used (Figure 6-2). Cross-hairs are manually positioned to points of interest on the image projected from the rear onto a ground glass screen. The X and Y coordinates are read from dials to the nearest 0.001 inch on the image, which is 5 inches by 7 inches on the screen (i.e., to 0.002 inch of the actual drop). The projection head is designed to accurately register the film as it is moved frame by frame; reference points in the image remain fixed to within a small error (probably a few thousandths of an inch). Shifting between forward to reverse directions of film transport causes a systematic shift of the image. Thus, the film must be run in one direction when coordinates on successive frames are to be compared.

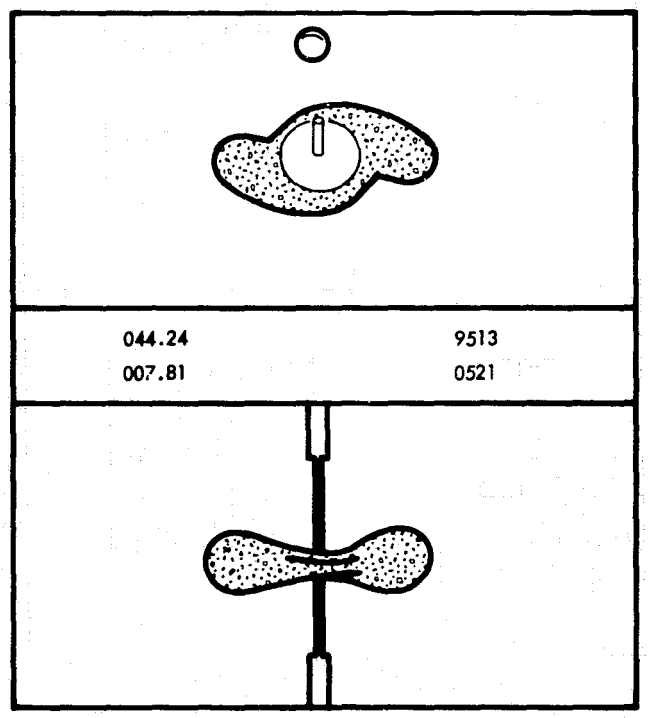

Figure 6-1. Film Format. The bottom and side views are seen in the same frame; the latter is upside down. Digital displays give (clockwise from upper left) the shaft period (multiplied by 100) (0.44 s), the film and run numbers (95 and 13), the date (5/21), and the time elapsed in the particular run (7.81 s).

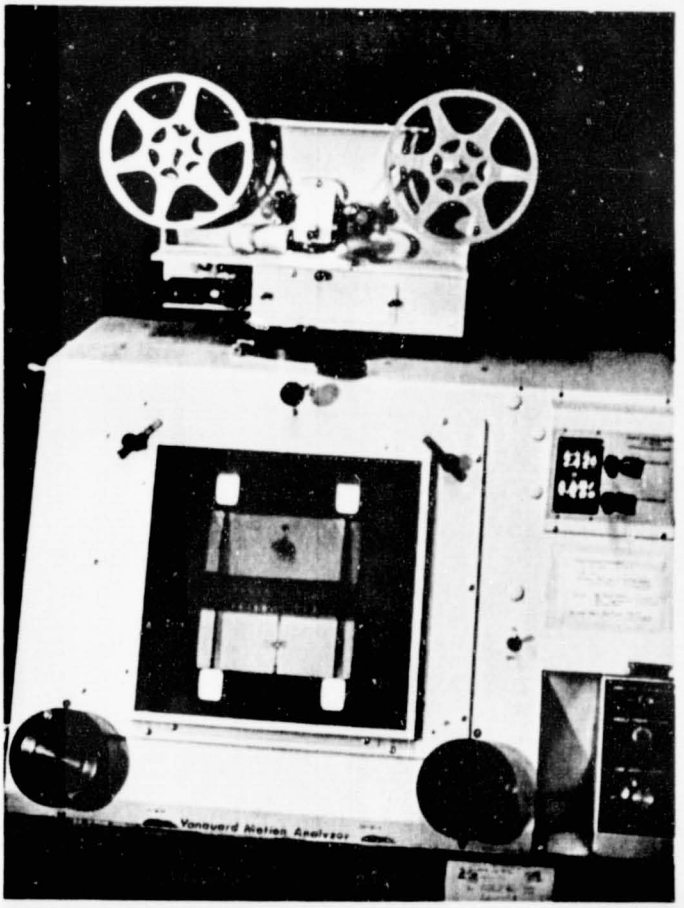

Figure 6-2. Vanguard Motion Analyzer

ORIGINAL PAGE IS
OF POOR QUALITY

SECTION VII

DATA ANALYSIS

A. AXISYMMETRIC SHAPE

The quantities which are determined for the axisymmetric shapes are a, the equatorial radius of the rotating drop, and Ω, the drop's angular velocity. From a the normalized cross-sectional area $A' = \pi a^2/a_o^2$ is calculated while Ω yields the dimensionless parameter $\Sigma = \Omega^2/(8\sigma/\rho a_o^3)$. In calculating Σ, ρ is the density of the oil (not the oil - mixture density difference, which is zero) and σ is the interfacial tension between the oil and mixture. a_o is computed from the calculated drop volume. The experimental axisymmetric values are determined from the maximum drop deformation for a given rotation velocity. The experimental values are presented in Figure 7-1. As Σ increases, the axisymmetric shapes become less stable with respect to the n=1 perturbation. Thus, no reliable data is available beyond the region where $\Sigma = 0.4$.

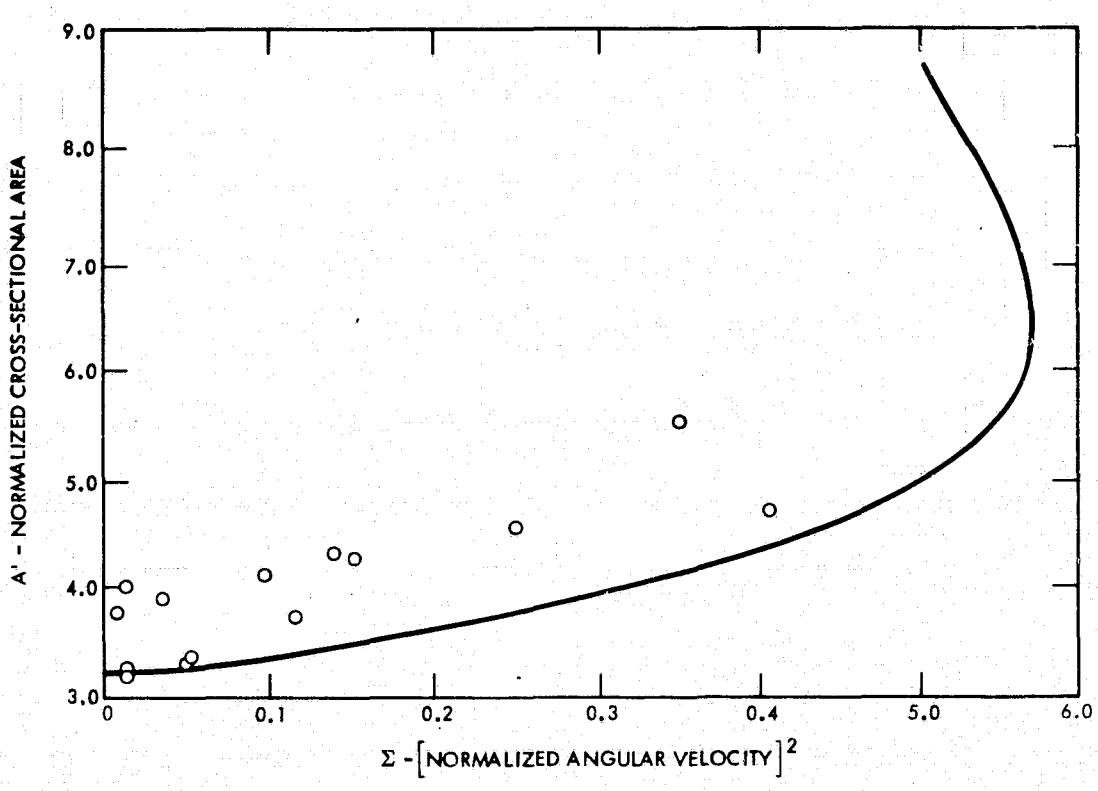

Figure 7-1. Experimental Results for Slowly Rotating Axisymmetric Drops. Theoretical Curve From Free Drop Calculations.[5,6,7]

B. NON-AXISYMMETRIC SHAPES

Figure 7-2 shows velocity profile data for a two-lobed shape; Figure 7-3 is a three-lobed shape. The existence of shear close to the disc is clearly demonstrated. It is also seen that at a position away from the disc where 90 percent of the mass is located a reasonably constant angular velocity exists. It is the measurement of this velocity which serves as the value for determining Σ for a given drop shape. However, the justification of this procedure is likely to break down during the initial spin up of the drop.

Figures 7-4 through 7-8 show graphs of the results of A/a_o^2 versus Σ for the drops which developed to two-lobed, three-lobed, and four-lobed shapes.

Unfortunately, the bifurcation points could not be accurately determined. However, the direction in which the A' versus Σ curve traversed in time is indicated on each graph. In each run, the drop remains axisymmetric for a time prior to developing into its lobed shape.

Figures 7-9 through 7-13 show the estimated angular momentum for all non-axisymmetric runs. All runs have been adjusted to have the same time origin. The curves for the two-lobed runs are qualitatively almost identical. However, for the three-lobed runs one run (45-48/12) peaks slightly later and at a higher value than the other. Comparison with the A' versus Σ curves shows that this run also peaks at a higher A' and lower angular velocity. Its shaft angular velocity is also lower than for the other three-lobed run. This may account for the later peaking in the angular momentum and the lower Σ values.

By looking at the A' versus Σ graphs of the three- and four-lobed runs, it can be seen that the curves occupy the same domain. This leads to the possibility that bifurcation points for the four-lobed shape and three-lobed shape are close, and the three-lobed shapes are more stable. As a result, the three-lobed shape occurred more frequently than the four-lobed shape.

The four-lobed curve of A' versus Σ also shows a rebound that is either nonexistent or not as profound in the three- and two-lobed runs.

In all runs the angular momentum increases initially, reaches a peak, and then decreases. The shaft angular velocity is constant in the critical region, before and after the lobes have fully developed.

Concerning the drop angular velocity versus time curves as shown in Figures 7-14 through 7-18, several interesting features stand out: 1) the angular velocity drops off sharply after the lobed shape has been fully developed, 2) the two-lobed run is of longer duration than the three- and four-lobed runs; and the three-lobed runs are likewise longer than the four-lobed run, 3) the rate of decrease of angular velocity is greater the larger the number of lobes; and 4) the rebound is evident in the early development of the four-lobed shape.

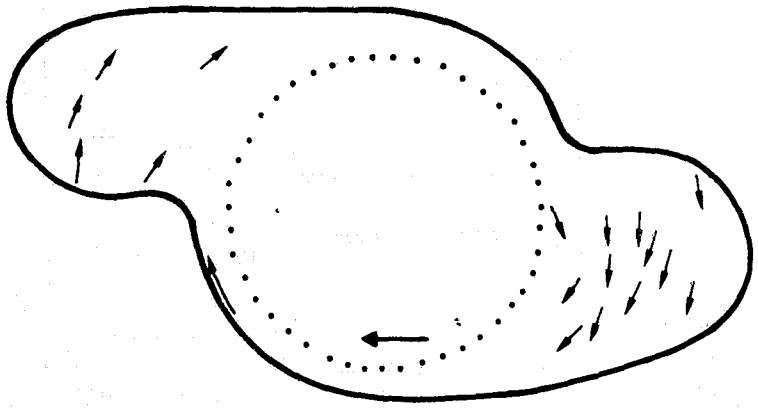

A) ANGULAR VELOCITY OF TRACERS WITHIN DROP

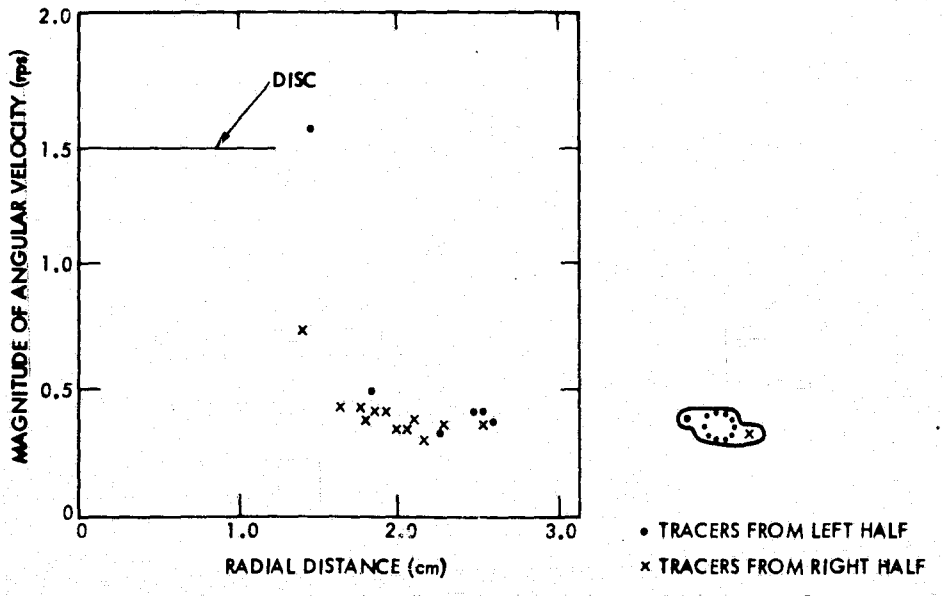

B) PROFILE OF ANGULAR VELOCITY AS A FUNCTION OF RADIAL DISTANCE

Figure 7-2. Angular Velocity Distribution for Two-Lobed Shape (Film 99-102, Run 8, 4.86 sec); $\Omega_{Drop} \sim 0.38$ rps and $\Omega_{Shaft} = 1.48$ rps

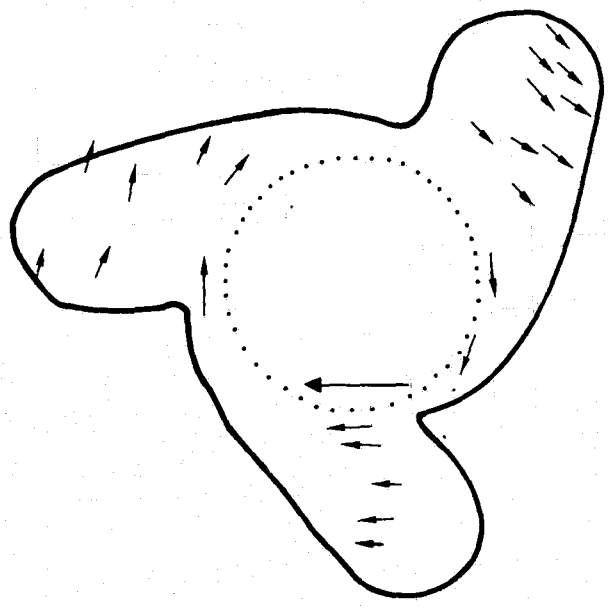

A. ANGULAR VELOCITY OF TRACERS WITHIN DROP

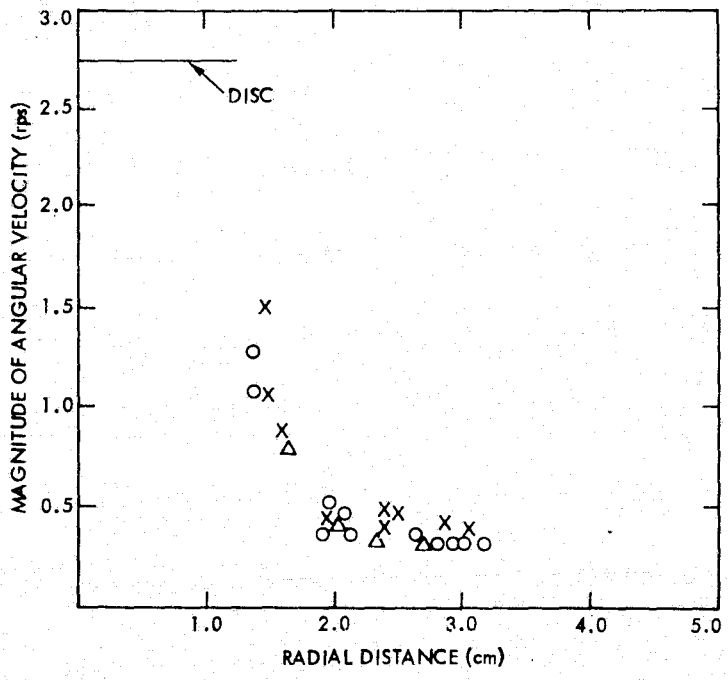

B. PROFILE OF ANGULAR VELOCITY AS A FUNCTION OF RADIAL DISTANCE

Figure 7-3. Angular Velocity Distribution for Three-Lobed Shape (Film 95-98, Run 16, 5.81 sec); $\Omega_{Drop} \sim 0.38$ rps and $\Omega_{Shaft} = 2.74$ rps

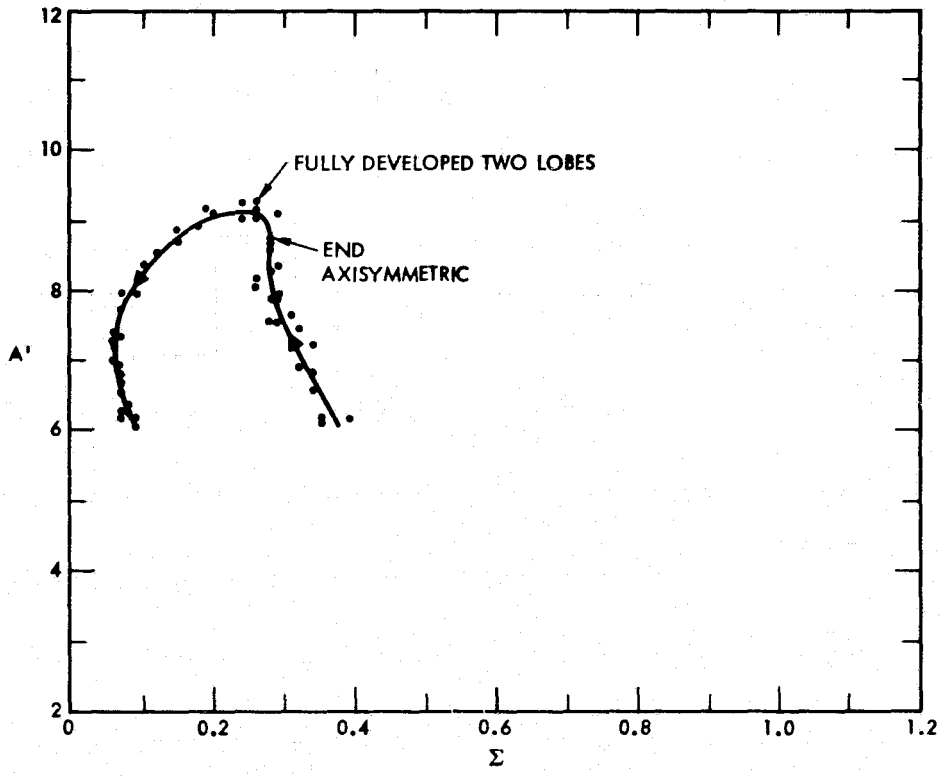

Figure 7-4. A' versus Σ for a Two Lobe Run (Film 95-98, Run 8) (A' is the normalized equatorial area and Σ is proportional to the square of the angular velocity).

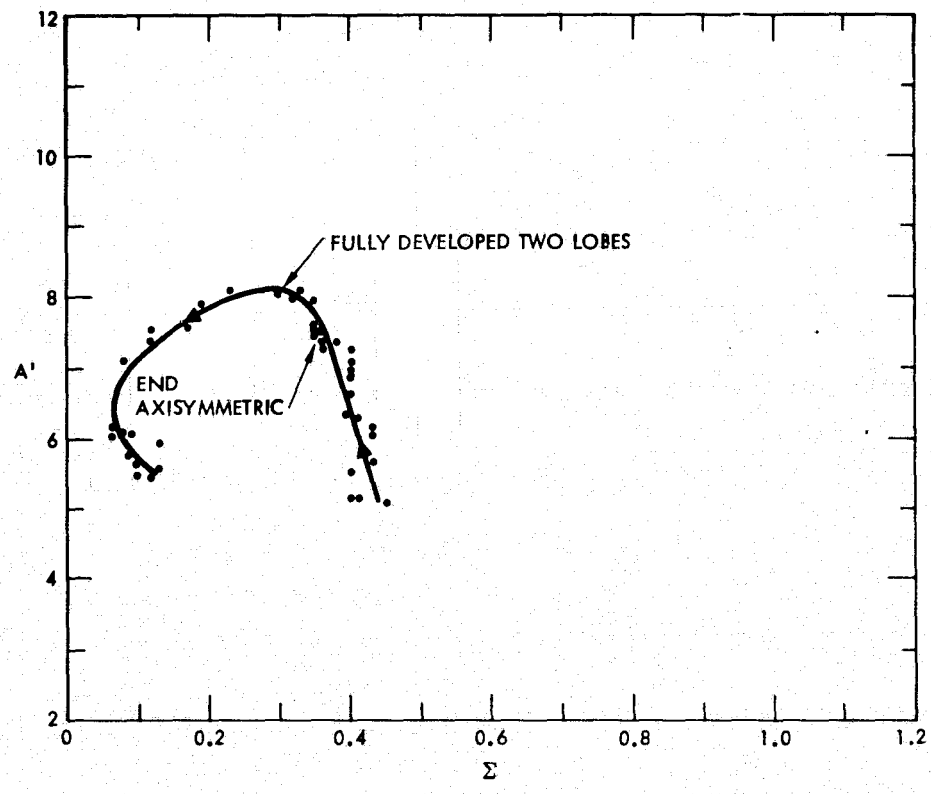

Figure 7-5. A' versus Σ for a Two Lobe Run, (Film 99-102, Run 8)

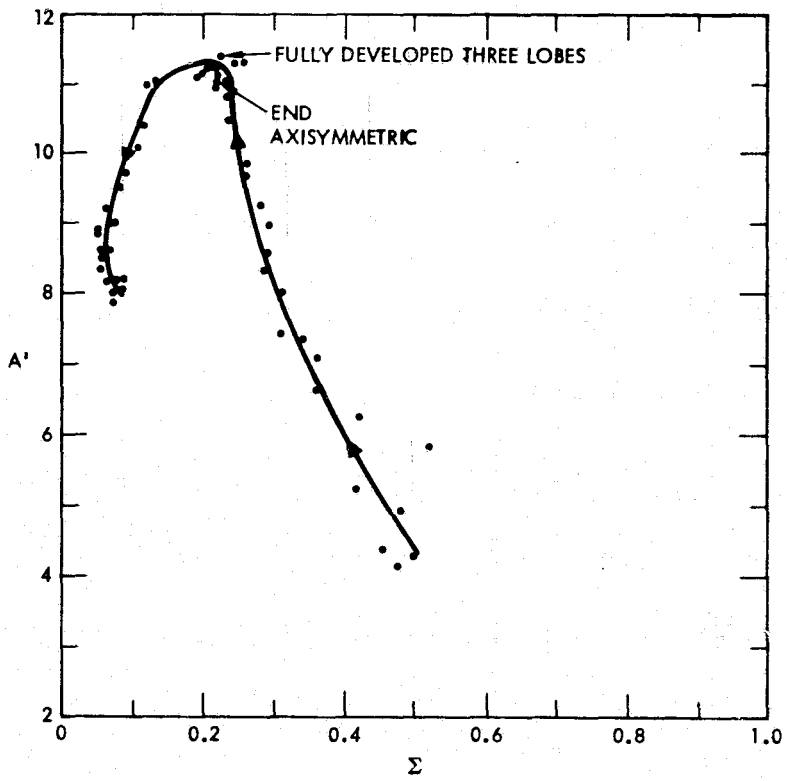

Figue 7-6. A' versus Σ for a Three Lobe Run, (Film 95-98, Run 12)

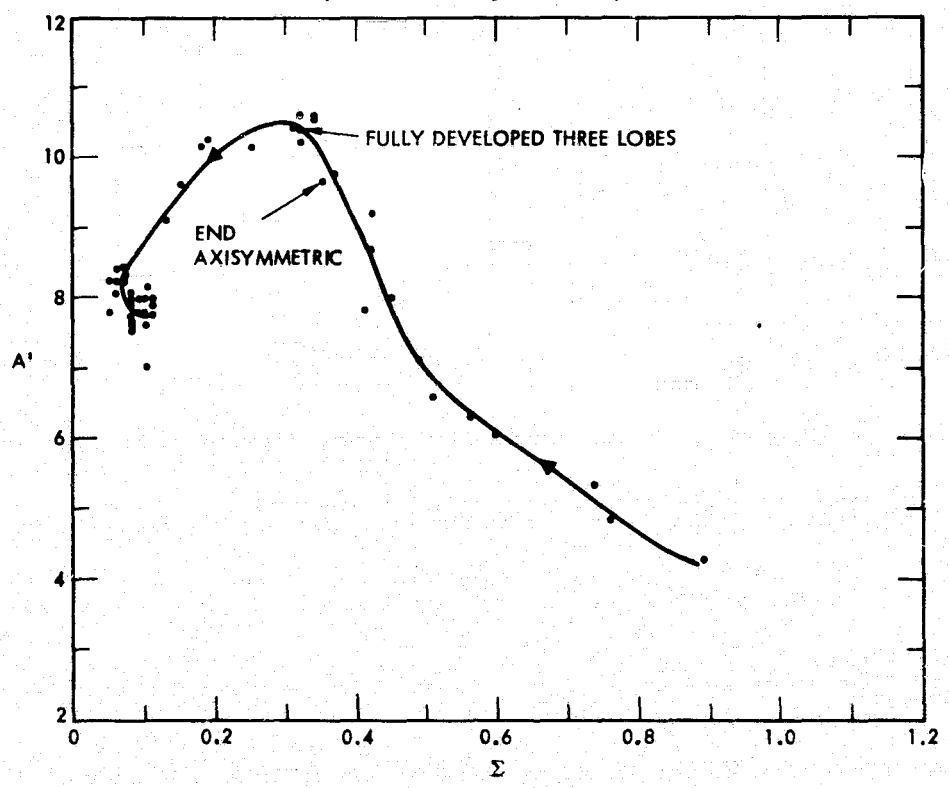

Figure 7-7. A' versus Σ for Three Lobe Run, (Film 103-106, Run 13)

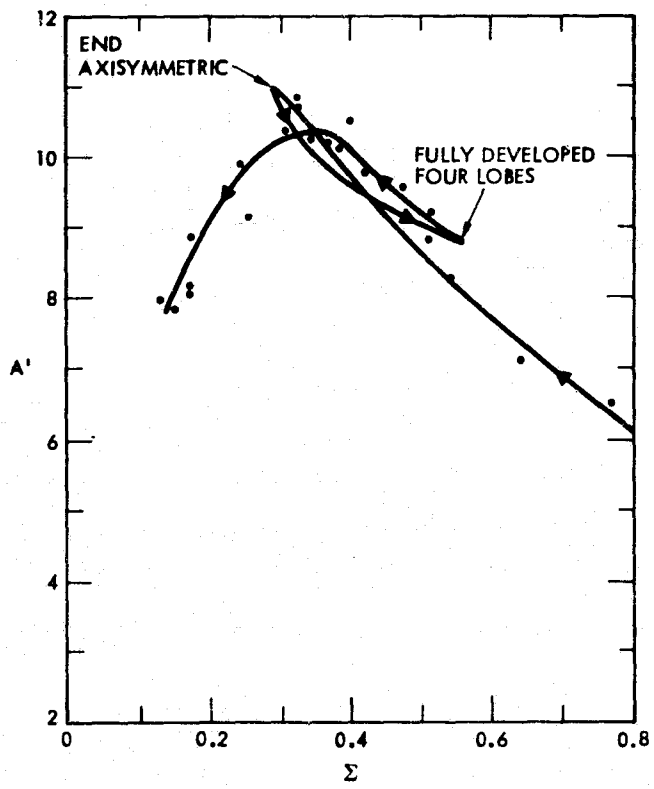

Figure 7-8. A' versus Σ for a Four Lobe Run, (Film 91-94, Run 21)

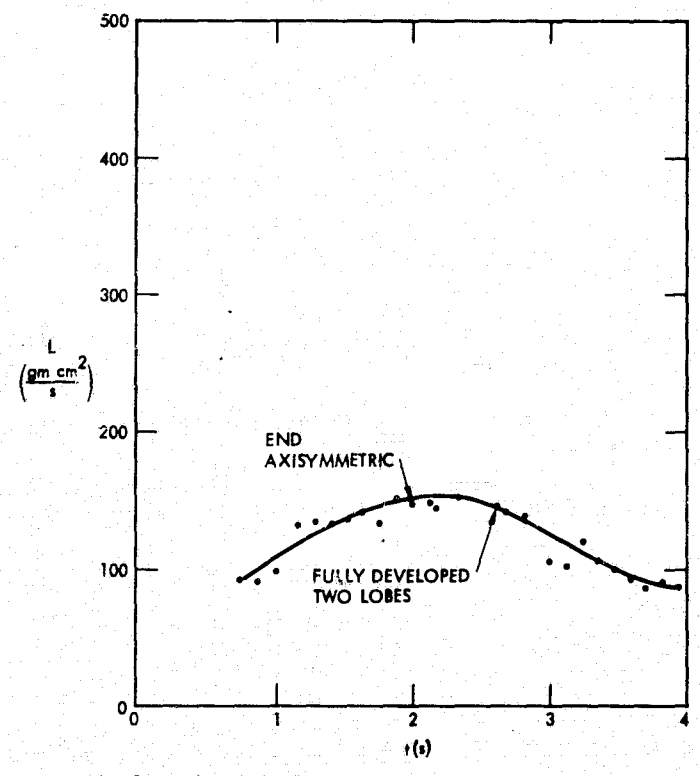

Figure 7-9. Angular Momentum Versus Time for a Two Lobe Run, (Film 95-59, Run 8)

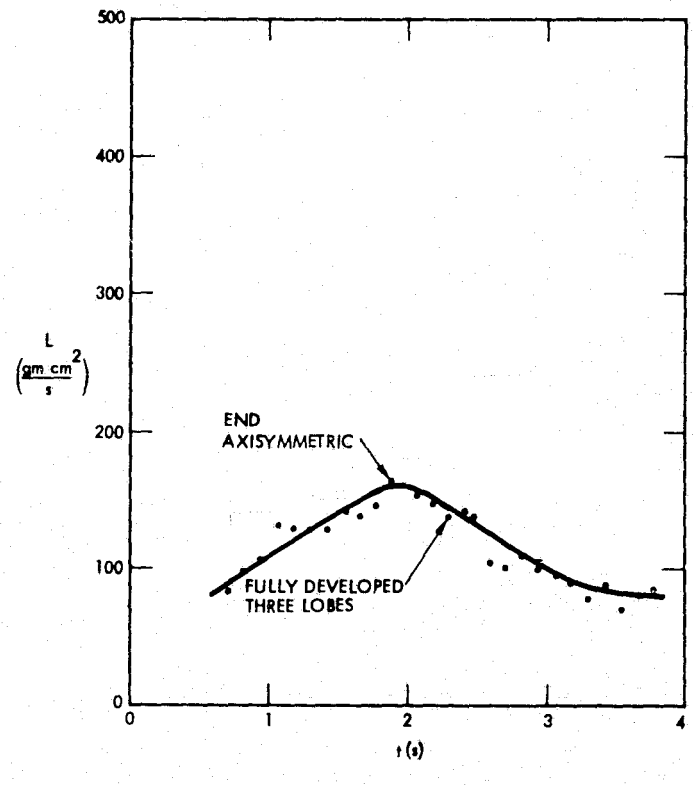

Figure 7-10. Angular Momentum versus Time for a Two Lobe Run, (Film 99-102, Run 8)

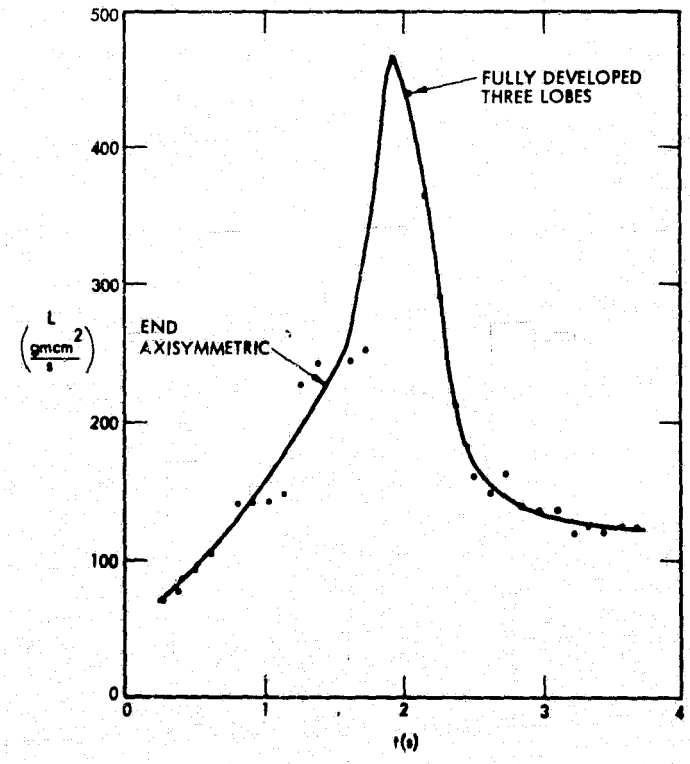

Figure 7-11. Angular Momentum versus Time for a Three Lobe Run, (Film 95-98, Run 12)

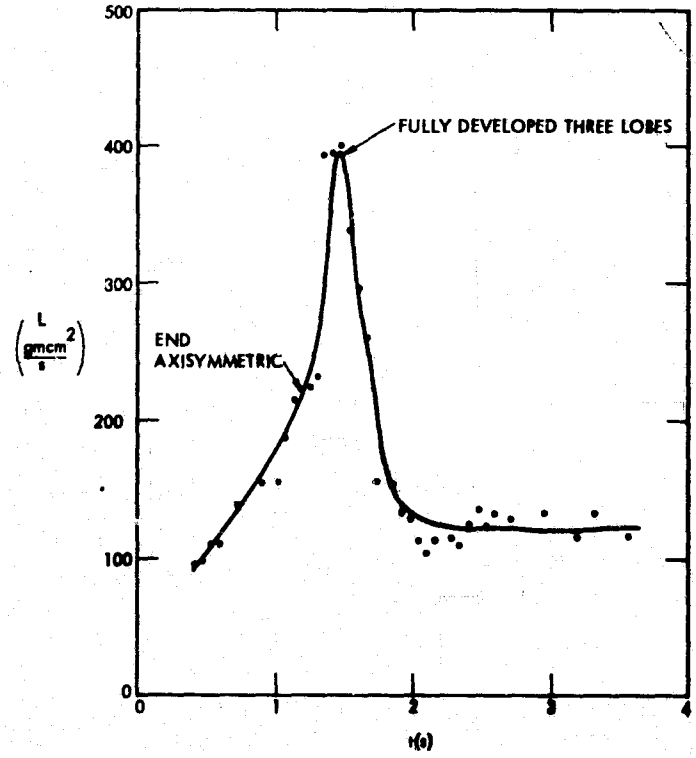

Figure 7-12. Angular Momentum versus Time for a Three Lobe Run, (Film 103-106, Run 13)

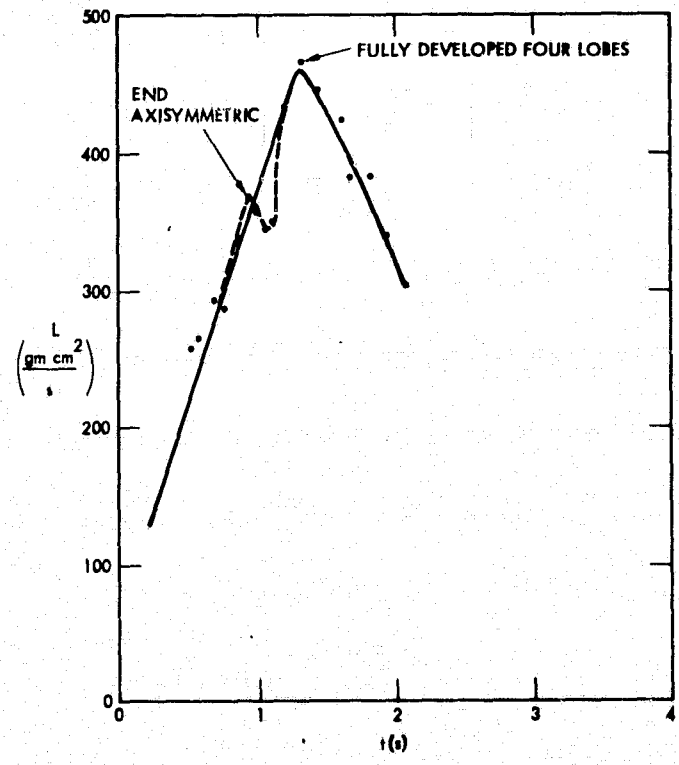

Figure 7-13. Angular Momentum versus Time for a Four Lobe Run, (Film 91-94, Run 21)

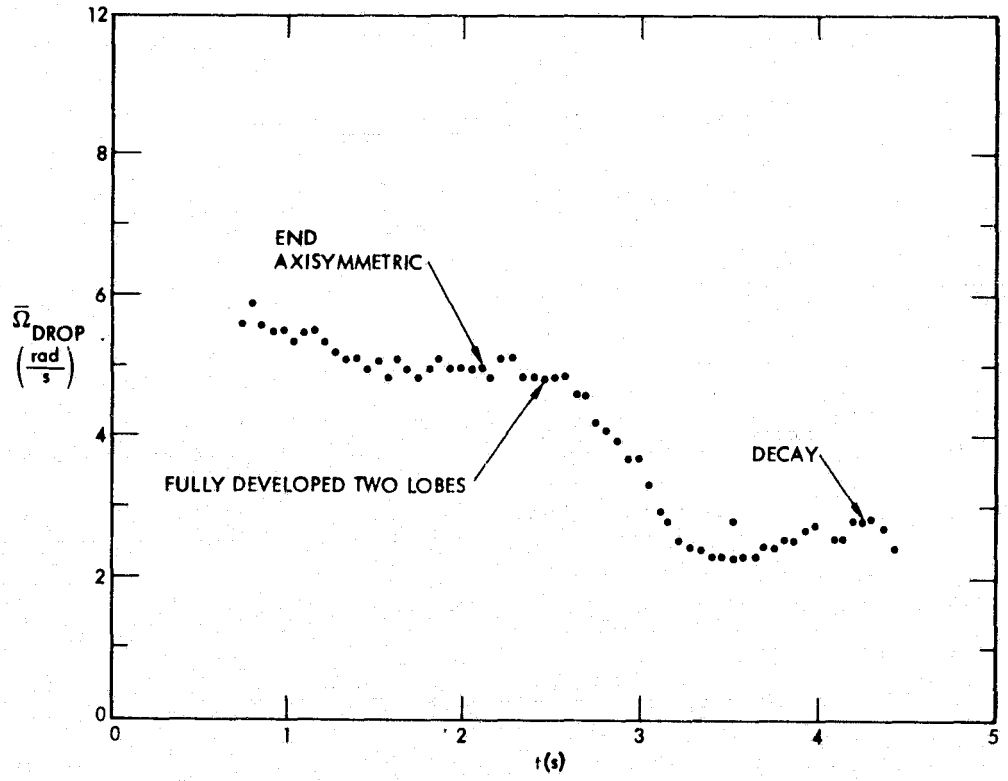

Figure 7-14. Drop Angular Velocity versus Time for a Two Lobe Run, (Film 95-98, Run 8)

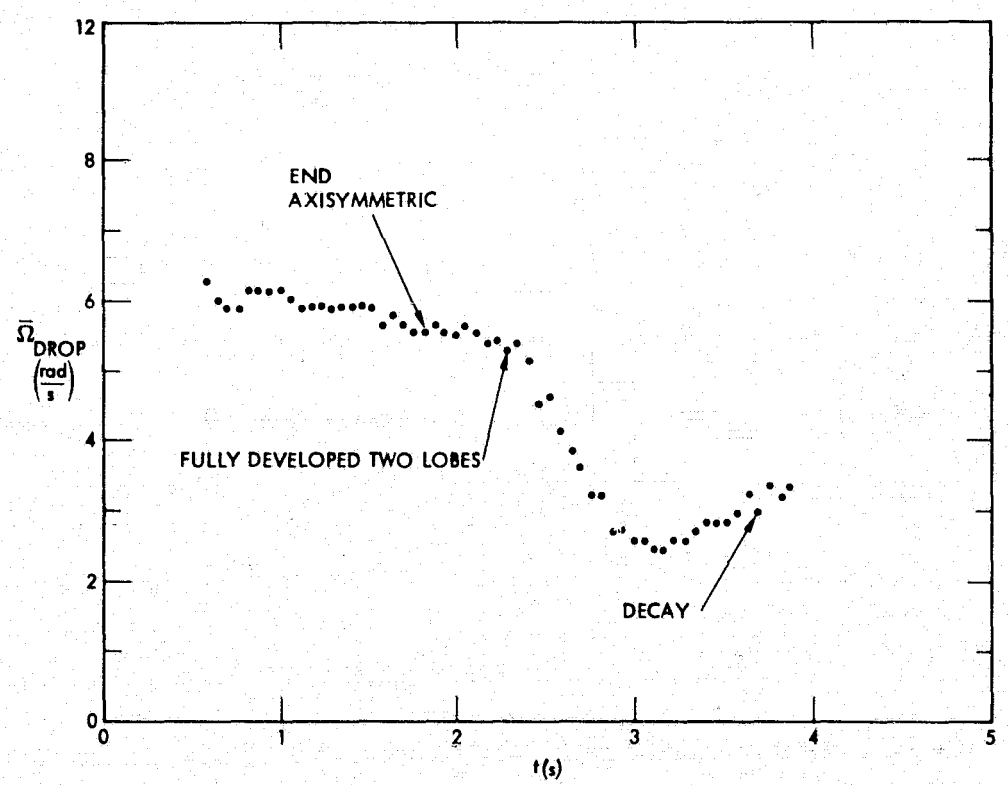

Figure 7-15. Drop Angular Velocity versus Time for a Two Lobe Run, (Film 99-102, Run 8)

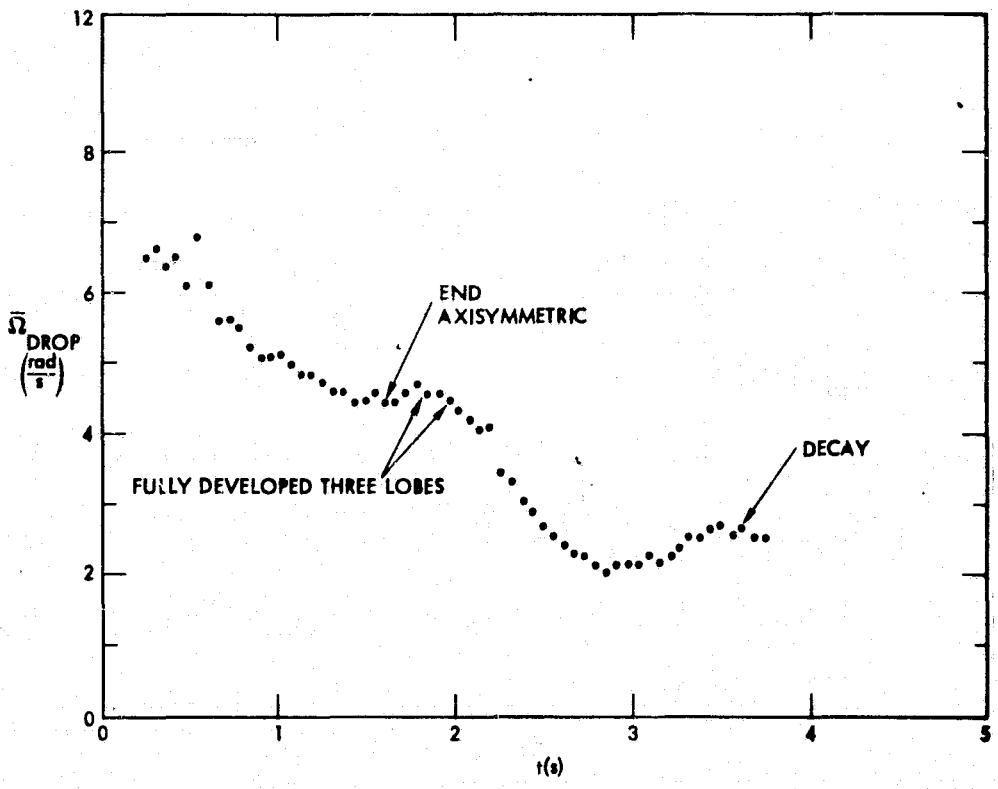

Figure 7-16. Drop Angular Velocity versus Time for a Three Lobe Run (Film 95-98, Run 12)

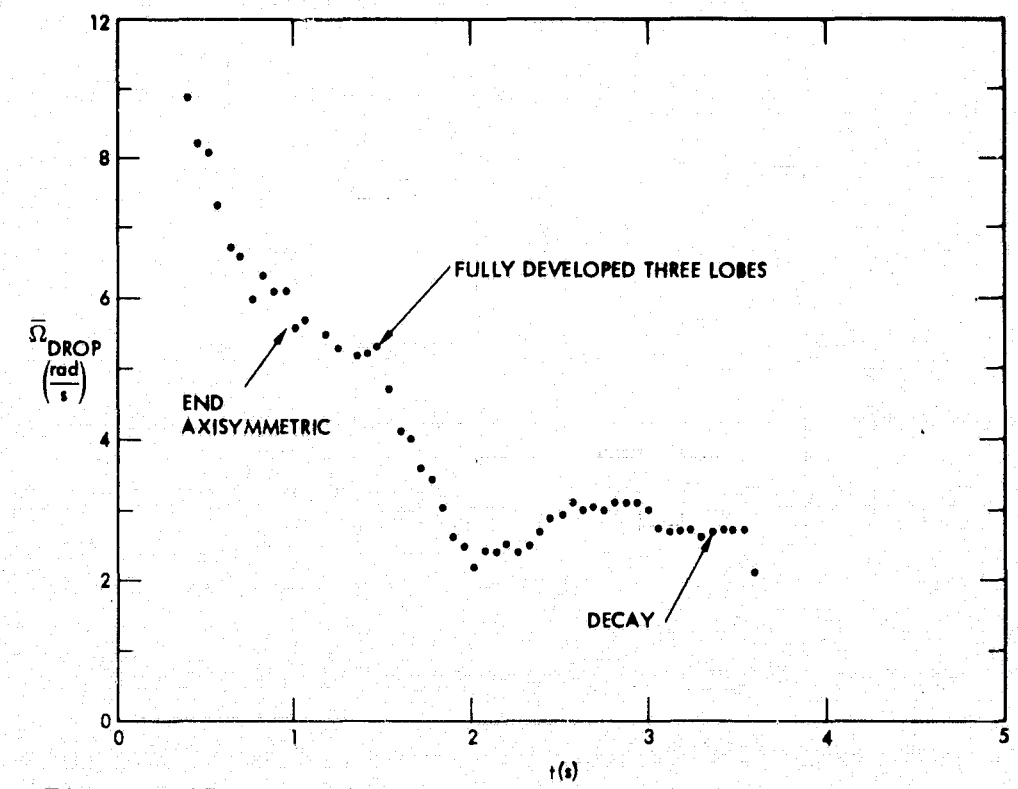

Figure 7-17. Drop Angular Velocity versus Time for a Three Lobe Run, (Film 103-106, Run 13)

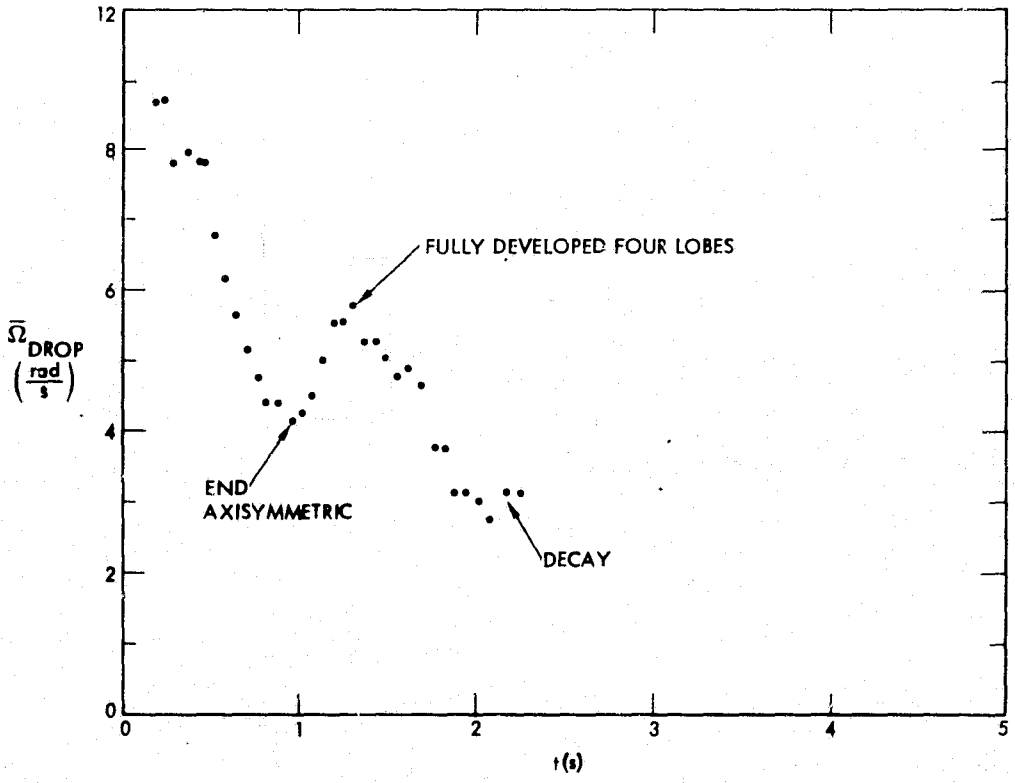

Figure 7-18. Drop Angular Velocity versus Time for a Four Lobe Run, (Film 91-94, Run 21)

SECTION VIII

CONCLUSIONS

Shapes of a rotating spheroid, including those reported by Plateau, have been observed and recorded in the JPL experiment. These include the flattening of slowly rotating drops and the generation of toroidal and lobed shapes at higher rotation rates. Using data recorded on movie film, the development and decay of the rotating shapes were studied for the first time. The neutrally buoyant tracer droplets allowed us to study the dynamics of the behavior, the secondary flow generated by the rotation, the interaction between the drop and the host liquid, and the coupling between the shaft and disc and the drop.

In the case of slowly rotating axisymmetric drops, direct comparisons of experiment with the theory of a free rotating drop were possible. The agreement between the two was surprisingly good; the qualitative shape of the equatorial area versus Σ curves were similar, only differing from theory by 30%. This is remarkable because the theory does not address the presence of an outer fluid. The generation and study of axisymmetric equilibrium shapes for higher rotation rates is difficult, because of the presence of the more stable $n = 1$ lobed nonaxisymmetric shape. This mechanism prohibited us from extracting from the data the exact location of the bifurcation points between families of equilibrium shapes.

When generating $n \geq 2$ lobed drops in a controlled manner, primarily two and three lobe shapes were obtained. The latter had not been observed before. The study of equilibrium configurations of these lobed shapes is made difficult by the presence of the outer fluid; as soon as the lobes occur, the interaction between the drop and the host liquid increases significantly and generates large secondary flows. The accelerated transfer of angular momentum from the drop in the lobed configurations gives rise to decay routes in which one lobe slows and is absorbed by the one trailing it; this continues until there is only one arm left. There were two exceptional types of decay in which either the whole drop would lift up (independent of the neutral buoyancy level) and become sessile on the disc, forming a slanted drop; in both of these two cases, the shapes were very stable and longlived. The behavior of lobed shapes was not easily compared to the free drop theory. The study of the angular velocities and momenta demonstrated that the development of the various lobed shapes takes similar paths, but no evidence was found for the location of branch points between axisymmetric and triaxial behavior.

One of the important parameters of this experiment which must be characterized is the surface force. The determination of interfacial surface tension is challenging when the densities of both liquids are close, and it becomes very difficult to use established techniques when they are identical in density. It is under just these conditions that information is required. Using the pendant drop method, the surface tension has been bracketed from above and below in density difference. New ways of narrowing the uncertainty are under investigation.

At present, no framework exists for describing the dynamics of a drop rotating in another liquid: it is the authors' hope that the various phenomena assembled in the course of this work will stimulate one.

SECTION IX

REFERENCES

1 J. Plateau, "Experimental and Theoretical Researches on the Figures of Equilibrium of a Liquid Mass Withdrawn from the Actions of Gravity," The Annual Report of the Board of Regents of the Smithsonian Institution (Government Printing Office, Washington, DC, 1863), p 207.

2a T. G. Wang, D. D. Elleman, and M. M. Saffren, "Dynamics of Rotating and Oscillating Free Drops: Investigation and Technical Plan," JPL Document 701-238 (June, 1976) (an internal document).

2b T. G. Wang, M. M. Saffren, and D. D. Elleman, "Drop Dynamics in Space," International Colloquium on Drops and Bubbles, Proceedings (Pasadena, CA, August 28-30, 1974), p. 266.

3 E. G. Gibson, "Skylab Fluid Mechanics Demonstrations," Ibid, p 158.

4 W. J. Swiatecki, "The Rotating, Charged or Gravitating Liquid Drop, and Problems in Nuclear Physics and Astronomy," Ibid., p 52.

5 R. Brown, "The Shape and Stability of Three-Dimensional Interfaces," PhD Thesis, University of Minnesota (Minneapolis, MN, 1979).

6 S. Chandrasekhar, "The Stability of a Rotating Liquid Drop," Proc. Roy. Soc. (London) 286 (1965), p 1.

7a D. K. Ross, "The Shape and Energy of a Revolving Liquid Mass Held Together by Surface Tension," Aust. J. Phys. 21 (1968), p 823.

7b Ibid., p 837.

8 P. E. Appell, Traite de Mecanique Rationelle, Vol. 4, Chapter 9 (Paris, Gauthier-Villars, 1932).

9 Lord Rayleigh, "The Equilibrium of Revolving Liquid Under Capillary Force," Phil. Mag 28 (1914), p 161.

10 D. Sperber, "Equilibrium Configuration and Fission Barrier for Liquid Drop Nuclei with High Angular Momentum," Phys. Rev. 130 (1962), p 468.

11 H. M. Princen, "The Equilibrium Shape of Interfaces, Drops, and Bubbles. Rigid and Deformable Particles and Interfaces," Surface and Colloid Science Vol. 3, edited by E. Matijevic (New York, NY, Wiley-Interscience, 1969).

12a J. R. Carruthers and M. Grasso, "Studies of Floating Liquid Zones in Zero Gravity," J. Appl. Phys. 43 (1972), p 436.

12b J. R. Carruthers and M. Grasso, "The Stabilities of Floating Liquid Zones in Simulated Zero Gravity," J. Crystal Growth 13/14 (1972), p 611.

13

References for the Physical Properties of Water/Methanol Mixtures

13a

A. E. Dunstan and F. B. Thole, "The Relation Between Viscosity and Chemical Constitution: Part IV. Viscosity and Hydration in Solution," J. Chem. Soc. 95 (1909), p 1556 (viscosity @ 20°, 25°, 30°C).

13b

U.S. National Bureau of Standards, Standard Density and Volumetric Tables, Circ. 19 (1924) (density @ 15°C).

13c

L. G. Longsworth and D. A. MacInnes, "Ion Conductances in Water-Methanol Mixtures," J. Phys. Chem. 43 (1939), p 239 (viscosity @ 25°C; ion conductances @ 25°C).

13d S. W. Subnis, W. V. Bhagwat, and R. B. Kanugo, "Application of Mixture Law to Rheochor - Part II," J. Indian Chem. Soc. 25 (1948), p 575 (density @ 30°, 40°, 50°C).

13e C. Carr and J. A. Riddick, "Physical Properties of Methanol-Water System," Ind. Eng. Chem. 43 (1951), p 692 (density @ 25°, 30°, 40°C; viscosity @ 25°C).

13f G. Clifford and J. A. Campbell, "Densities in the Methanol-Water System at 25.00°C," J. Am. Chem. Soc. 73 (1951), p 5449 (density @ 25°C).

13g S. Z. Mikhail and W. R. Kimel, "Densities and Viscosities of Methanol-Water Mixtures," J. Chem. Eng. Data 6 (1961), p 533 (density and viscosity @ 30°, 35°, 40°, 50°C).

13h H. A. Neidig, R. T. Yingling, K. L. Lockwood, and T. G. Teates, "Interaction in Chemical Systems I. The Methanol-Water System," J. Chem. Educ. 42, (1965), p 309; "Interaction in Chemical Systems II. The KCl-Methanol-Water System," J. Chem. Educ. 42 (1965), p 368 (volume change, apparent molar volume, enthalpy of solution).

13i National Research Council, International Critical Tables, Vol. 7 (McGraw-Hill, New York, NY, 1930) (index of refraction @ 15°, 15.5°, 17°, 25°C).

13j J. L. R. Morgan and M. Neidle, "The Weight of a Falling Drop and the Laws of State, XVII. The Drop Weights, Surface Tensions and Capillary Constants of Aqueous Solutions of Ethyl, Methyl, and Amyl Alcohols and of Acetic and Formic Acid," J. Am. Chem. Soc. 35 (1913), p 1856 (density and surface tension @ 30°C).

14 W. D. Harkins and T. F. Anderson, "A Simple Accurate Film Balance of the Vertical Type for Biological and Chemical Work, and a Theoretical and Experimental Comparison with the Horizontal Type," J. Am. Chem. Soc. 59 (1937), p 2189.

15a J. M. Andreas, E. H. Hauser, and W. B. Tucker, "Boundary Tension for Pendant Drops," J. Phy. Chem. 42, (1938), p 1001.

15b R. J. Roe, V. L. Baccheta, and P. M. A. Wong, "Refinement of Pendant Drop Method for the Measurement of Surface Tension of Viscous Liquid," J. Phys. Chem. 71 (1967), p 4190.

16a W. D. Harkins and F. E. Brown, "The Determination of Surface Tension (Free Surface Energy), and the Weight of Falling Drops: the Surface Tension of Water and Benzene by the Capillary Height Method," J. Am. Chem. Soc. 41 (1918), p 499.

16b W. D. Harkins and H. F. Jordan, "A Method for the Determination of Surface and Interfacial Tension from the Maximum Pull on a Ring," J. Am. Chem. Soc. 52 (1930), p 1751.

16c C. Huh and S. G. Mason, "A Rigorous Theory of Ring Tensiometry," Colloid Polymer 253 (1975), p 566.

17 L. S. B. Cammack, "A Report on the Measurement of the Interfacial Tension Between Silicone Oil and Water-Methanol Mixtures at 25°C," Preliminary Report, JPL Containerless Processing Group (June, 1979) (an internal document).

18a B. Vonnegut, "Rotating Bubble Method for the Determination of Surface and Interfacial Tensions," Rev. Sci. Inst. 13 (1942), p 6.

18b H. M. Princen, I. Y. Zia, and S. G. Mason, "Measurement of Interfacial Tension from the Shape of a Rotating Drop," J. Colloid Interface Sci. 23 (1967), p 99.

19a W. G. Hyzer, Photographic Instrumentation Science and Engineering, U.S. Gov't. Printing Office, Washington, DC (1965).

19b B. R. Clayton and B. S. Massey, "Flow Visualization in Water: A Review of Techniques," J. Sci. Instrum. 44 (1967), p 2.

APPENDIX A

THEORETICAL VALUES FOR DROP EQUILIBRIUM SHAPES

Sources:

a) S. Chandrasekhar - Proc. R. Soc., A286, 1 (1965)

b) D. Ross - Aust. J. Phys., 21, 8 (1968)

c) R. Brown - Ph.D Thesis, Univ. of Minn. (1978)

d) D. Sperber - Phys. Rev., 130, 468 (1963)

Parameters:

Σ = angular velocity parameter = $\Omega^2 \left(\frac{\rho a_o}{8\sigma}\right)^3$

r'_{max} = equatorial radius $/a_o$

A' = equatorial area $/a_o^2$

U' = surface energy $/E_o$

T' = kinetic energy $/E_o$

ε' = total energy $/E_o$

I' = moment of inertia $/I_o$

L' = angular momentum $/L_o$

where

a_o = radius of resting drop

ρ = density of drop

σ = interfacial surface tension

E_o = surface energy of spherical drop of radius a_o
$= 4\pi\sigma a_o^2$

I_o = moment of inertia of sphere
$= \frac{2}{5}\left(\frac{4}{3}\pi a_o^3\right) \rho\, a_o^2$

$L_o = \sqrt{I_o\, E_o}$

a) Chandrasekhar[6]

Σ	r'_{max}	A'	U'	T'	ε'	I'	L'
0.1393	1.050	3.4636		0.0821		1.1043	0.4257
0.1748	1.0640	3.5566		0.1059		1.1358	0.4905
0.2176	1.0819	3.6773		0.1326		1.1764	0.5585
0.2719	1.1061	3.8436		0.1790		1.2341	0.6646
0.3425	1.1425	4.1007		0.2421		1.3254	0.8011
0.5000	1.2599	4.9868		0.4451		1.6692	1.2190
0.5679	1.4485	6.5915		0.7835		2.4250	1.9493
0.5400	1.5716	7.7595		0.8934		3.1020	2.3543
0.5000	1.6701	8.7626		1.0079		3.7795	2.7602

b) Ross[7]

Axisymmetric Drop

Σ	r'_{max}	A'	U'	T'	ε'	I'	L'
0.000	1.000	3.142	1.000	0.000	1.000	1.000	0.000
0.338	1.140	4.082	1.032	0.237	1.269	1.319	0.791
0.500	1.260	4.987	1.113	0.445	1.558	1.670	1.219
0.565	1.385	6.026	1.248	0.644	1.892	2.137	1.659
0.568	1.430	6.420	1.308	0.708	2.016	2.335	1.818
0.551	1.537	7.419	1.475	0.850	2.325	2.893	2.218
0.500	1.670	8.762	1.724	1.008	2.732	3.780	2.760

Toroidal Drop

Σ	r'_{max}	A'	U'	T'	ε'	I'	L'
0.040	4.126	10.163	2.62	0.65	3.27	30.469	7.194
0.102	2.206	7.800	1.90	0.47	2.37	8.606	2.847
0.203	1.674	6.603	1.63	0.46	2.09	4.259	1.995
0.325	1.445	5.968	1.39	0.46	1.85	2.655	1.569
0.476	1.326	5.469	1.23	0.46	1.69	1.812	1.404
0.476	1.281	5.140	1.14	0.46	1.60	1.812	1.249
0.490	1.225	4.711	1.11	0.44	1.55	1.684	1.210

c) Brown[5]

Axisymmetric							
Σ	r'_{max}	A'	U'[a]	T'	ε'	I'	L'
0.00	1.000	3.142	1.00	0.000	1.00	1.000	0.000
0.05	1.017	3.250	1.00	0.028	1.03	1.035	0.239
0.10	1.035	3.366	1.01	0.057	1.06	1.072	0.350
0.20	1.074	3.626	1.01	0.124	1.13	1.159	0.536
0.22	1.083	3.684	1.01	0.138	1.14	1.179	0.571
0.24	1.092	3.745	1.01	0.154	1.16	1.200	0.607
0.26	1.101	3.808	1.02	0.169	1.18	1.222	0.643
0.28	1.110	3.873	1.02	0.186	1.20	1.244	0.680
0.30	1.120	3.942	1.03	0.203	1.23	1.269	0.718
0.32	1.130	4.015	1.03	0.221	1.24	1.294	0.756
0.34	1.141	4.091	1.03	0.240	1.26	1.322	0.811
0.36	1.152	4.173	1.04	0.260	1.29	1.352	0.838
0.38	1.164	4.259	1.04	0.280	1.31	1.384	0.881
0.40	1.177	4.353	1.05	0.303	1.34	1.419	0.927
0.42	1.191	4.454	1.06	0.326	1.38	1.457	0.975
0.44	1.205	4.564	1.07	0.352	1.41	1.500	1.027
0.46	1.221	4.687	1.08	0.380	1.45	1.548	1.084
0.48	1.239	4.826	1.09	0.410	1.49	1.603	1.147
0.50	1.260	4.987	1.10	0.445	1.53	1.670	1.219
0.52	1.284	5.182	1.11	0.486	1.58	1.752	1.305
0.54	1.316	5.437	1.14	0.536	1.66	1.863	1.414
0.55	1.336	5.610	1.16	0.569	1.71	1.940	1.486
0.56	1.365	5.852	1.20	0.613	1.79	2.052	1.586
0.565	1.387	6.045	1.22	0.647	1.85	2.147	1.666
0.568	1.413	6.270	1.23	0.684	1.89	2.258	1.758

d) Sperber[b]

Σ	r'_{max}	A'	U'	T'	ε'	I'	L'
0.000	1.000	3.142	1.000	0.00	1.000	1.000	0.000
0.356	1.120	3.941	1.021	0.239	1.270	1.316	0.794
0.500	1.260	4.988	1.114	0.447	1.627	1.678	1.225
0.577	1.375	5.940	1.222	0.713	1.963	2.070	1.713
0.557	1.531	7.364	1.489	0.912	2.401	2.907	2.302
0.499	1.691	8.983	1.764	1.028	2.792	3.891	2.828

[a] Taken from graph F.8 (by A.P.C.)

[b] As noted by Chandrasekhar, Sperber's data is incorrect in places because he used too large a value for Σ_{max}.

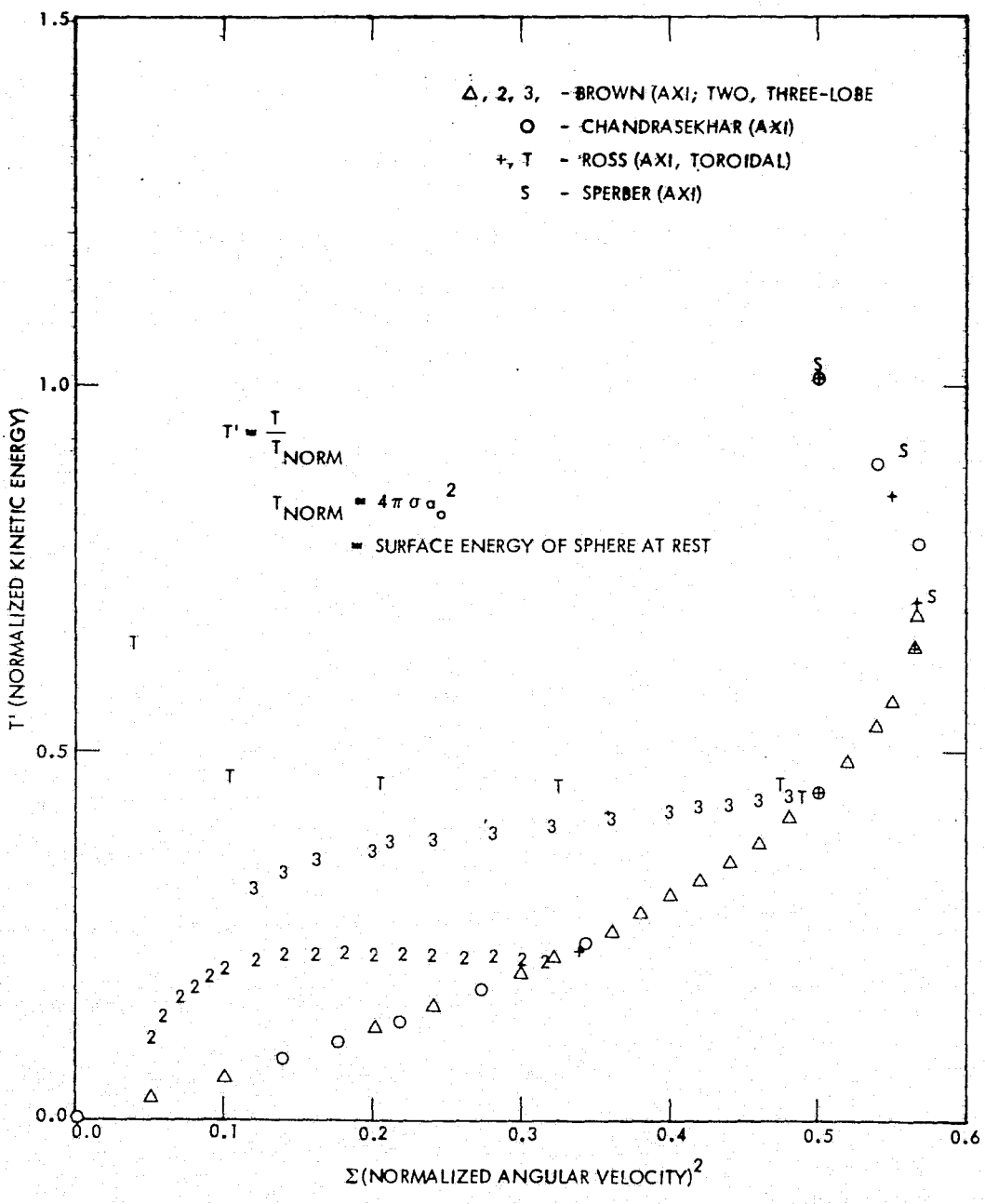

Figure A-1. Theoretical Calculations of Kinetic Energy versus Σ[5,6,7]

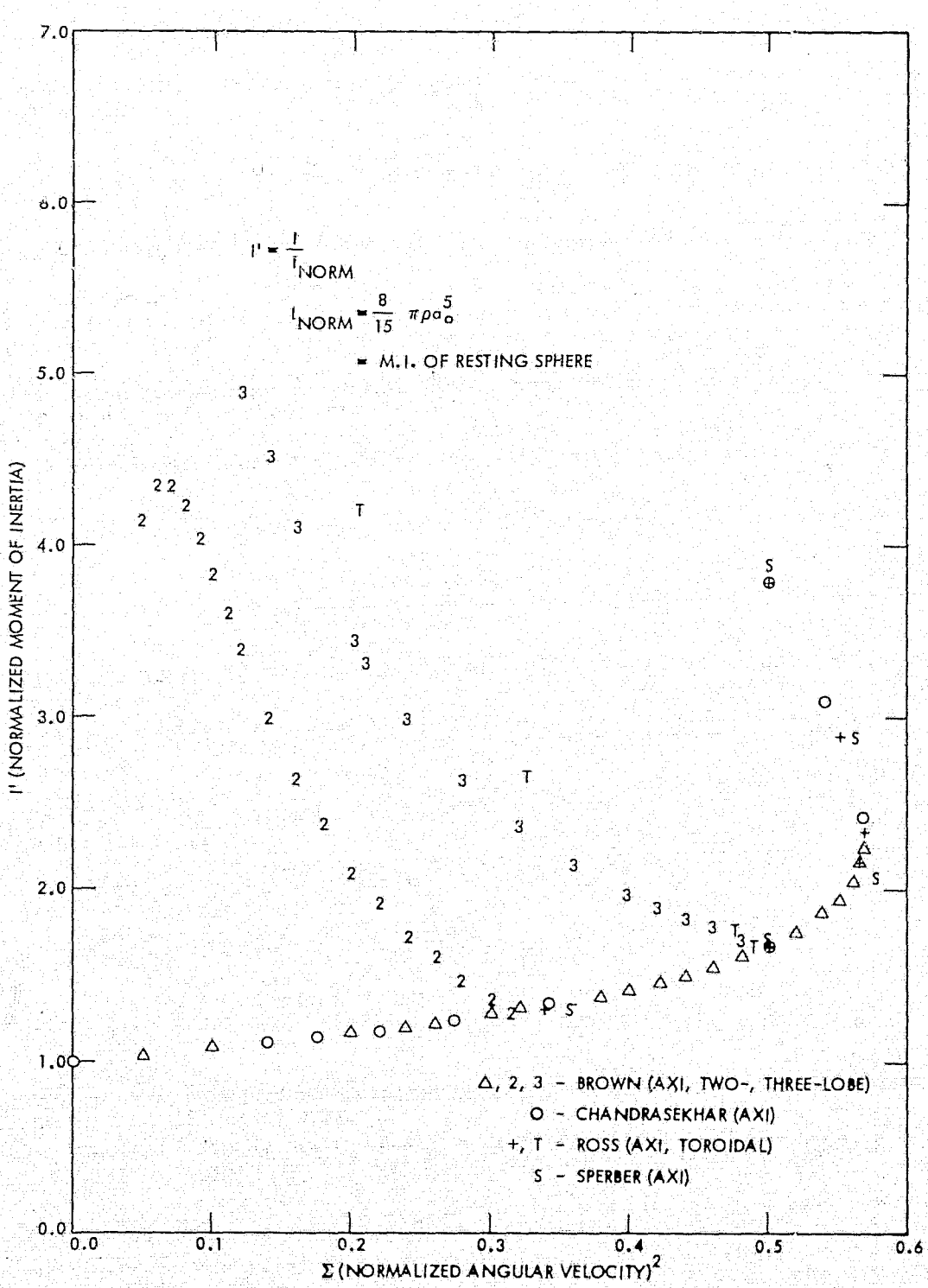

Figure A-2. Theoretical Calculations of Moment of Inertia versus [5,6,7]

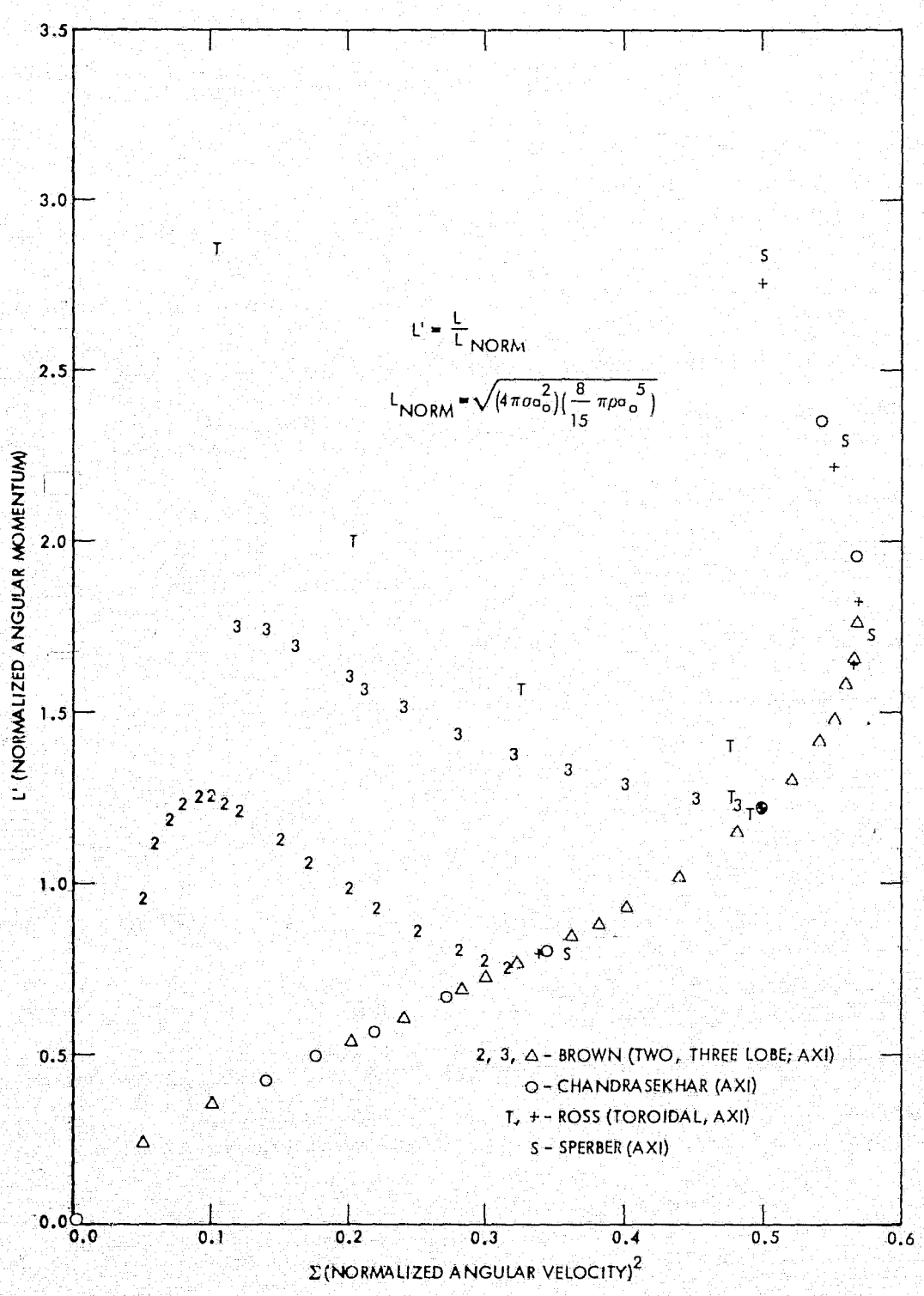

Figure A-3. Theoretical Calculations of Angular Momentum versus [5,6,7]